Coordination between stabilizing circuits and updating circuits in spatial orientation working memory

Rui Han[1], Hsuan-Pei Huang[2], Wan-Ju Lee[2], Chia-Lung Chuang[3], Hung-Hsiu Yen[2], Wei-Tse Kao[2], Hui-Yun Chang[2], and Chung-Chuan Lo[1,2,4,5,*]

[1]Institute of Bioinformatics and Structural Biology, National Tsing Hua University, Hsinchu, 30013, Taiwan

[2]Institute of Systems Neuroscience, National Tsing Hua University, Hsinchu, 30013, Taiwan

[3]Institute of Biotechnology, National Tsing Hua University, Hsinchu, 30013, Taiwan

[4]Brain Research Center, National Tsing Hua University, Hsinchu, 30013, Taiwan

[5]Lead Contact

*Correspondence: cclo@mx.nthu.edu.tw

Summary

Spatial orientation plays a crucial role in animal navigation. Recent studies of tethered *Drosophila melanogaster* (fruit fly) in a virtual reality setting showed that the orientation is encoded in the form of an activity bump, i.e. localized neural activity, in the torus-shaped ellipsoid body (EB). Moreover, a fly can maintain working memory of its orientation with a stable and persistent activity bump in the absence of any visual cue, and update the memory in accordance with changes of the body orientation by shifting the location of the bump. Although the neural circuit that is responsible for shifting the bump has been extensively studied lately, how the nervous system shifts the bump while maintains its stability and persistence is poorly understood. We investigated this question using free moving fruit flies in a spatial orientation memory task, and manipulated two EB subsystems, the P circuit, which has been suggested for the stabilization function, and the C circuit, which has been suggested for the updating function but was largely overlooked. We discovered that overactivating either circuit produced distinct behavioral deficits, confirming that the two circuits play important but different roles in the orientation working memory. Furthermore, suppressing either circuit disrupted the memory, suggesting that the C or P circuit alone is not sufficient to maintain the orientation working memory. We reproduced the observations with a spiking neural network model of EB and demonstrated that spatial orientation working memory requires coordinated activation of the stabilizing and updating neural processes in different movement modes.

Keywords

Central complex, ellipsoid body, spatial orientation memory, working memory, Buridan's paradigm, *Drosophila melanogaster*

Introduction

Maintaining spatial orientation is a crucial cognitive capability required for animal navigation [1,2], and understanding the detailed neural mechanisms of spatial orientation is of great interest to researchers in the fields of neurobiology [3–5] or neuromorphic engineering [6–8]. In recent years, significant progress has been made in identifying the neural circuits that support spatial orientation [9] in the central complex of *Drosophila melanogaster* [10,11]. The central complex has long been associated with short-term spatial memory, visual pattern memory, and motor control [12,13]. The recent discovery of head-direction [14] selectivity and localized neural activity (the activity bump) in two central complex neuropils, the ellipsoid body (EB) and the protocerebral bridge (PB), has also linked the central complex to the function of spatial orientation [9,10].

In light of these empirical observations, several neural circuit models of the central complex have been proposed to elucidate the neural circuit mechanisms of head-direction selectivity or other functions associated with the central complex [15–17]. However, if we consider the situation when the animals are required to navigate in the absence of any landmark, the underlying neural mechanisms appear to be more complex. Under this condition, the animals need to maintain working memory about the spatial orientation. On one hand, models of working memory emphasize the maintenance of stable and persistent neural activity (the activity bump) [18]. On the other hand, models of spatial orientation describe how the position of the activity bump can be shifted and updated in accordance with changes of the head direction [16,17,19]. It is not clear how these two seemly contradicting mechanisms work together to support spatial orientation working memory.

Recently, a model of the EB-PB circuits proposed in Su et al., (2017) was built strictly based on connectomic data and provided a detailed picture of the neural circuit interactions underlying spatial orientation and its working memory [15]. The model suggests the involvement of two sets of coupled circuits that connect the EB and PB. One set that consists of EIP (or E-PG) and PEI neurons forms symmetric recurrent connections, and the other set that consists of EIP and PEN (or P-EN) forms asymmetric recurrent

connections [20,21]. The symmetric circuit, named the C circuit in this paper, forms an attractor network and is proposed to support the formation of the activity bump and to stabilize it, while the asymmetric circuit, named the P circuit in this paper, forms a shifter network and is proposed to shift the bump position in accordance with changes in body orientation. The model successfully demonstrated the angular errors when a fly moved in darkness [22] and predicted the asymmetric activity in the PB during rotation [23]. Furthermore, the model made an important and unique prediction: the function of spatial orientation working memory requires activation of both C and P circuits.

However, previous experimental studies on the head-direction selectivity of fruit flies were conducted with tethered flies in a virtual reality setting, and these studies mainly focused on how the P circuit updates the head direction by performing angular integration. It is not clear whether this circuit plays roles in spatial orientation memory in free-moving flies with a more realistic behavioral setting. It is also not clear whether other neurons such as those in the C circuit also play roles as predicted in Su et al., (2017). In the present study, we aimed to address these questions and designed a behavioral task of spatial orientation working memory based on the classic Buridan's paradigm [24–27]. Previous studies have demonstrated that the activity bump is driven by the visual stimulus when the landmark is visible [20,22,28,29]. This evidence suggests that the role of the C and P circuits may be more important when no landmark is available because the circuits need to support the activity bump without the aid of visual stimuli. Therefore, we manipulated the C-ring and P-ring neurons, which are two types of GABAergic neurons presumably inhibiting the downstream C and P circuits [6,30], and investigated the impacts on the behavior of the fruit flies for both landmark available and landmark absent conditions. We also simulated the behavioral task using the EB-PB model [15]. The model produced altered neural activities that were consistent with the behavioral changes observed in the fruit flies with different experimental conditions. The present study provides a novel picture on how coordinated activation that alternated between the stabilizing and updating neural processes play a crucial role in the spatial orientation working memory.

Results

Spatial orientation working memory

To investigate the mechanism of spatial orientation working memory in *Drosophila melanogaster*, we first developed a behavioral task based on Buridan's paradigm [24,26,27] (see Methods) (Figures 1A, 1B, and S1) and submitted wild-type flies to the test. The task consisted of three stages. In the first (pre-stimulus) stage, in which no visual landmark was presented, the fruit flies walked randomly without any preferred orientation (Figure 1C) and spent most of the time walking along the edge of the arena (Figure S1). In the second (stimulus) stage, in which two landmarks appeared at 0° and 180° on the screen, the flies exhibited significant visual fixation behavior by expressing a strong preference for walking back and forth between the two landmarks and spent less time walking along the edge (Figure 1D). This stage tested the ability of flies to orient themselves toward visual landmarks, and no memory was required. In the third (post-stimulus) stage, in which the landmarks disappeared, we found that the flies still maintained a behavior preference similar to that in the second stage, although with a weaker tendency of fixation (Figure 1E). The ability of visual fixation in this stage indicated successful recall of the landmark directions with respect to the fly's momentary heading, and is therefore an indication of spatial orientation working memory. To determine the duration of memory and whether it is dependent on the stimulus (landmarks) exposure time, we conducted the task using different durations of the stimulus stage and calculated the performance index (PI) as a function of time. Two interesting properties were discovered; first, the duration of memory is positively correlated with the stimulus exposure time (Figures 1F and 1J), and second, the memory is unexpectedly long considering the stimulus duration was shorter than that used in previous studies [22,25]. The spatial orientation memory could be maintained for up to 40 s following a 120 s of stimulus exposure (Figures 1I and 1J).

We further quantified the quality of the memory in the post-stimulus stage by calculating the fixation strength and the fixation deviation angle (STAR Methods). The former indicated the strength (or the specificity) and the latter indicated the accuracy of the

128 memory. Note that during the post-stimulus stage, the flies always exhibited fixation
129 behavior (shaded period in Figures 1F-1I) not immediately, but a short period after the end
130 of the stimulus stage (Table S1). We analysed the fixation strength and deviation angle for
131 the periods before and during the fixation behavior in the post-stimulus stage and found
132 that the flies exhibited a significantly lower strength in the pre-fixation period than in the
133 fixation period.
134
135 **Impairment of spatial orientation working memory by suppressing ring neurons**
136 Next, we investigated how suppressing the C or P circuits affected spatial orientation
137 memory in the behavioral task. The manipulation was performed via the C-ring (R1 ring)
138 neurons and P-ring neurons [6], which project from the lateral triangle to the entire C- and
139 P-rings, respectively. The ring neurons were reported to be GABAergic [31], and hence
140 presumably exhibited suppression over the downstream C circuit (EIP and PEI neurons)
141 or P circuit (EIP and PEN neurons). Previous studies have reported the roles of ring
142 neurons in visually-guided behavior [32–34]. However, the roles of ring neurons in the
143 working memory of spatial orientation in the presence or absence of visual cues remain
144 unclear. We separately suppressed the C-ring and P-ring neurons, and observed the
145 impact on behavior. We used the same behavioral paradigm as described in the previous
146 section with a 60 s stimulus stage.
147 We suppressed the ring neurons by hyperpolarizing the membrane (*;;UAS-Kir2.1*) [3]
148 or by blocking synaptic transmission (*;;UAS-TNT*) [3] (STAR Methods). For C-ring neuron
149 (Figure 2A) suppression, we found that both methods led to similar behavioral changes.
150 While the flies with suppressed C-ring neurons exhibited the same PI as did the wild-type
151 flies during the stimulus stage (Figure 2B), the PI of the flies with suppressed C-ring
152 neurons decreased significantly during the post-stimulus stage and was markedly lower
153 than that of the wild-type flies (Figure 2C).
154 The PI plots described above provide information regarding the frequency of
155 movement toward the landmarks versus toward the perpendicular directions. However, it
156 is also important to investigate the overall movement patterns of the flies in all directions.

157 Therefore, we present the radar plots, which indicate the frequency of movement toward
158 all angles in 12-quantiles (each quantile represents a range of 30°). Inspection of the
159 movement trajectories (Figure 2D) and the radar plots of the wild-type flies and the flies
160 with suppressed C-ring neurons (Figure 2E) revealed that the suppression produced a
161 small effect in the stimulus stage, indicating that the flies largely maintained their fixation
162 behavior. However, the effect was markedly more profound during the post-stimulus stage.
163 To obtain a more detailed overview of the effect, we plotted the radar plots for four
164 different time windows of the post-stimulus stage (Figure 2F). We discovered that while
165 the wild-type flies exhibited a slight deviation from the actual landmark direction (Figures
166 2F top row, and S3A), flies with suppressed C-ring neurons exhibited a profound change
167 in the movement direction during the post-stimulus stage (Figures 2F bottom row, and
168 S3B and S3C). This deviation increased with time (Table S2). Flies that underwent two
169 different methods of C-ring neuron suppression exhibited similar deviation rates, which
170 were markedly larger than that of the wild-type flies (Figure 2G).

171 We next investigated the behavioral changes involving suppression of the P-ring
172 neurons using the same methods as used for the C-ring neurons (Figure 3A). Whereas
173 both methods of P-ring neuron suppression led to similar behavioral changes, they were
174 distinct from those led by C-ring neuron suppression. With suppression of P-ring neurons,
175 the PI of the flies decreased significantly in both the stimulus and post-stimulus stages
176 (Figures 3B and 3C). By inspecting the movement trajectories and the radar plots, we
177 discovered that the flies with suppressed P-ring neurons moved randomly during the
178 stimulus stage (Figure 3D) and the post-stimulus (Figures 3E, and S4A and S4B).

179 One may argue that the loss of fixation behavior in flies with suppressed P-ring
180 neurons was not the result of impairment in spatial orientation but was due to deficiencies
181 in other functions such as locomotion or vision. To investigate whether the motor function
182 was normal, we measured the activity level (percentage of movement bouts in the given
183 period) and speed (mean movement speed in the movement bouts) in the flies with
184 suppressed P-ring neurons in the pre-stimulus stage. We compared the result with that of
185 wild-type flies and did not discover significant differences between the wild-type flies and

186 the flies with suppressed P-ring neurons (Table S3). Next, we conducted the vision test
187 (STAR Methods) for the flies with suppressed P-ring neurons. We measured the escape
188 rate for the approaching laser beam (STAR Methods) and found no significant difference
189 between the wild-type flies (81.82%) (Video S1) and the flies with suppressed P-ring
190 neurons (80.95%) (Video S2), while the escape rate of the fruit flies with deficient
191 photosensors (genotype: *;;ninaE*) (Video S3) was 0%, suggesting that P-ring neuron
192 suppression did not impair vision.
193
194 **Impairment of spatial orientation working memory by activating ring neurons**
195 We have inspected the effect of the ring neuron suppression, which presumably
196 overactivated the downstream circuits. But how about suppression these downstream
197 circuits? In particular, if we temporally suppress the circuits, would orientation memory
198 interrupt? To this end, we activated the C-ring or P-ring neurons by optogenetics using two
199 temporal protocols (STAR Methods) (Figures 4 and S5). For C-ring neuron
200 photoactivation during the last 30 s of the stimulus stage, the movement speed and
201 activity level of the flies significantly reduced during this period (Table S3; Video S4), and
202 the fixation behavior in the post-stimulus stage was also shortened to only 10 s (Figures
203 4A and 4B). The result indicated that orientation working memory is interference by
204 photoactivation of the C-ring neurons during the stimulus stage. When the photoactivation
205 was applied midway during the post-stimulus stage (20-30 s), the flies lost the fixation
206 behavior after the photoactivation (Figures 4C and 4D). For P-ring neuron photoactivation
207 during the last 30 s of the stimulus stage, the speed and activity level of the flies were
208 closed to that of the wild-type flies (Table S3; Video S5), and the fixation behavior during
209 the activation period and the post-stimulus stage remained intact (Figures 4E and 4F).
210 However, photoactivating the P-ring neurons during the 20-30 s of post-stimulus stage
211 abolished the subsequent fixation behavior (Figures 4G and 4H), an effect that is identical
212 to that of the C-ring activation during the same period (Figures 4C and 4D).
213
214 **Hypothesis of the underlying neural mechanisms**

To summarize the results of the behavioral and neural functional tests, we plot schematics that compared the movement patterns of wild-type flies and flies with C-ring or P-ring neuron manipulation in all three stages (Figure S2). The wild-type flies exhibited strong fixation behavior toward the landmark directions during the stimulus stage. The fixation behavior was still strong but with a slight deviation in the fixation direction during the post-stimulus stage, indicating the presence of working memory of the landmark direction (Figure S2A). Flies with photoactivation of P-ring neurons during the stimulus stage performed similarly (Figure S2A). Flies with suppressed C-ring neurons also exhibited a strong preference but with a slightly deviated direction during the stimulus stage (fig. S2B). The deviation increased progressively during the post-stimulus stage, suggesting that the flies maintained the memory of the existence of the landmarks but with incorrect memory of their orientation. In contrast, the flies with suppressed P-ring neurons did not exhibit fixation behavior in both stages, indicating that these flies lost spatial orientation regardless of whether the cue was visible (Figure S2C). Flies with photoactivation of C-ring neurons during the stimulus stage exhibited markedly weakened fixation behavior in both activation period and the post-stimulus stage (Figure S2D). Finally, short photoactivation during the post-stimulus stage of either C-ring or P-ring neurons both led to abolished fixation behavior after the activation period (Figure S2E).

The behavioral results can be used to examine the hypothesis of the neural mechanisms proposed in the EB-PB model [15], which suggests that the C and P circuit activate alternately between the forward movement and rotation states. According to the model, the P-ring neurons activate and suppress the P circuit (EIP / PEN) during forward movement such that the C circuit is allowed to perform its function by stabilizing the activity bump in EB (Figure 5A). In contrast, during rotation the C-ring neurons activate and suppress the C circuit (EIP / PEN) such that the P circuit can update (shift) the bump location in accordance with the changing head direction (Figure 5B). To illustrate how manipulating the C-ring or P-ring neurons affect the orientation memory, we plot activation tables for each experimental condition (Figures 5C-5G). The tables indicate whether the C circuit (EIP / PEI) or the P circuit (EIP / PEN) activates during rotation or forward

movement under the given experimental condition. For wild-type flies, C circuit and P circuit only activates during forward movement and rotation, respectively (Figure 5C). For the ring neuron suppression experiments, the suppression leads to overactivation of the downstream C or P circuits. Based on the model hypothesis, overactivation of the C circuit interferes bump shifting during rotation (Figure 5D). In the stimulus stage, such an interference does make a major impact on the behavior because the activity bump is driven by the visual landmarks and still accurately reflects the true landmark location. However, when the landmark is not available during the post-stimulus stage, such an interference makes a significant impact on bump shifting so that the flies cannot track their orientation accurately. The bump still exists, so that the flies can still perform fixation behavior, but with inaccurate orientation. In contrast, if P circuit is overactivated, it interferes the function of the C circuit and destabilizes the bump (Figure 5E). Based on the EB-PB model, the P circuit can be divided into two subcircuits with one that shifts the bump in the clockwise direction and the other that shifts the bump in the counterclockwise direction. Therefore, overactivated P circuit attempts to shift the bump in both directions, leading to a diffused bump that eventually spreads the neural activity across the entire ring. As a result, the flies lost their orientation no matter whether the visual landmarks are available or not.

For photoactivation of the ring neurons, we assume that the activation leads to suppression of the downstream C or P circuits. Therefore, C-ring neuron photoactivation affects forward movement while P-ring neuron photoactivation affects rotation movement (Figures 5F and 5G). In the affected movement periods, both C and P circuits do not function and the EB loses its activity bump completely when the visual landmark is absent. As a result, the flies lose their orientation memory after the photoactivation during the post-stimulus stage. However, if the photoactivation is applied during the stimulus-stage, the bump is weakened but not completely lost because it can still be driven by the visual stimulus (landmark). As a result, the activity bump is maintained in most trials during the post-stimulus stage and the flies are able to perform fixation behavior. This argument is verified by the model simulations as shown in the next section.

273

274 **The computational model of spatial orientation working memory**

275 We have illustrated in Figure 5 that how interrupted functionality of the C or P circuits
276 affected the spatial orientation working memory. Next, we further demonstrated such
277 neural mechanisms using the EB-PB model [15] by performing the model simulations
278 based on the same experimental protocols used in the present study.

279 The simulations based on the default model parameters corresponded to the
280 wild-type files. The simulated wild-type flies were able to maintain activity bump in both
281 stimulus and post-stimulus stages as expected (Figure 6A). The model with suppressed
282 C-ring neurons still exhibited a robust activity bump (Figure 6B) in both stimulus and
283 post-stimulus stages. In contrast, the model with suppressed P-ring neurons lost the
284 activity bump (Figure 6C). For C-ring neuron suppression, the manipulation did not seem
285 to interrupt the bump. However, the C-ring neuron suppressed model was less accurate in
286 tracking the landmark locations than the simulated wild-type flies during the post-stimulus
287 stage. This is consistent with experimental observations (Figures 2F and 2G). A statistical
288 analysis is shown and described later in Fig. 6I. For P-ring neuron suppression, the loss of
289 activity bump in both stages is consistent with the loss of orientation observed in
290 experiments (Figure 3).

291 Next, we simulated the photoactivation experiments in the model. The C-ring neuron
292 activation during the last 30 s of the stimulus stage produced an unstable bump during the
293 stimulus stage. As a result, in about 43% of the trials the model lost the activity bump
294 completely during the post-stimulus stage (Figure 6D). The result is consistent with the
295 significantly weaker fixation behavior observed in experiments (Figures 4A and 4B). For
296 C-ring neuron activation during the post-stimulus stage, the activity bump disappeared
297 completely after the photoactivation (Figure 6E), leading to a loss of orientation as
298 observed in experiments (Figures 4C and 4D). Interestingly, P-ring neuron photoactivation
299 in the model during the stimulus stage did not seem to make a major impact on the bump
300 stability and the bump in the majority (~79%) of the trials was successfully maintained in
301 the post-stimulus stage (Figure 6F). In contrast, photoactivation of P-ring neurons during

302 the post-stimulus stage abolished the bump completely (Figure 6G). The stimulation
303 results of the P-ring photoactivation are also consistent with the empirical observations
304 (Figures 4E-4H).

305 For the neural manipulation that did not disrupt the activity bump in the model, the
306 bump location may still deviate from the actual head direction. In fact, naturally occurred
307 deviation between the bump location and the true head direction in wild-type flies was
308 observed in previous experiments [22]. This is also true in the model simulation in the
309 present study (Figure 6H). We further investigated such deviation in the condition of
310 C-ring neuron suppression and found that during the post-stimulus stage, the deviation
311 between the bump and the true heading was significantly larger than that of the simulated
312 wide-type flies (Figure 6I), and this result is consistent with the experiments (Figure 2F).
313 We also investigated the deviation for the simulated P-ring neuron photoactivation and
314 found the deviation was not significantly larger than that of the simulated wild-type flies
315 (Figure 6I). The result is also consistent with the experiments (Figures 2F, 2G, and 4F).
316

Discussion

In the past few years, studies have demonstrated that the P circuit related neurons (PEN & EIP) play a crucial role in tracking the virtual head direction in tethered fruit flies [15,20,21]. In the present study, we tested spatial orientation working memory of free moving fruit flies using a behavioral task, and discovered that in addition to the P circuit, properly functioned C circuit is also crucial for the memory. Manipulation of either circuit through the ring neurons led to different behavioral abnormality in the task. By performing computer simulations on a previously proposed EB-PB neural circuit model, we were able to explain the results of the experiments and provided a novel and detailed working hypothesis of the neural circuit mechanism underlying spatial orientation working memory. In the hypothesis, the memory is maintained through two alternately activated neural processes: one that stabilizes the position of the activity bump and one that updates the position of the bump. The former is activated when a fruit fly maintains a steady head direction and the latter is activated when the fly rotates its body. Overactivating or suppressing either process disrupts the alternation of the two processes and therefore leads to incorrect or even loss of orientation memory.

There are a few more interesting discoveries worth discussing. We discovered that although suppressing C-ring neurons did not affect the ability of the flies to orient themselves toward the visual landmarks when they were visible, after they were turned off, the flies exhibited fixation behavior with progressively increasing deviation from the true directions of the landmarks. This result suggested that although the flies remembered the existence of the landmarks and attempted to fixate on them, their memory of the directions of the landmarks was inaccurate. Such interpretation implies the segregation of the neural mechanisms of orientation memory regarding the “where” and “what” of a landmark.

We also discovered an unexpectedly long duration of spatial orientation working memory during the post-stimulus stage in which the landmarks were invisible. Previous studies reported the occurrence of post-stimulus fixation behavior that lasted only for a few seconds immediately following the offset of the landmarks [25]. However, we observed that the flies resumed their fixation behavior later and maintained it for a longer

period. This fixation behavior, which characterized the orientation memory of the landmarks, has a duration that is linearly proportional to the duration of visual stimulus exposure. The reason underlying the brief interruption of fixation behavior in the beginning of this stage is unclear. However, this interruption could be due to a “startle” effect owing to the sudden disappearance of the landmarks. Further studies are needed to investigate this point.

Several other important questions remain to be addressed. Current experimental evidence suggested that the activity bump represents the fly’s sense of orientation in a similar manner to that of the head-direction system found in rodents [14]. However, in the present work, in order to perform the fixation behavior after the landmarks disappeared, the flies need to remember the existence of the landmarks. It remains unclear whether this memory is stored in another neural circuit and the EB merely provides a reference frame for orientation regardless of the locations of the landmarks, or whether the activity bump in the EB represents the actual memory of the landmarks. This question leads to another related issue regarding the content of the orientation memory, which may consist of two components: One representing the fly’s memory of the position of a certain reference point in space, and the other representing the fly’s memory of the positions of the objects (landmarks) with respect to the reference point. The current experimental setup is not able to address this issue. A novel task that can disassociate these two components is required for further investigation.

In conclusion, the present work reveals the detailed neural mechanisms of spatial orientation memory in three aspects. First, the experiment revealed the distinct roles of the C-ring and P-ring neurons in spatial orientation working memory. Second, the result of C-ring neuron suppression implies disassociation of the “where” and “what” components of the memory. Third, the study supports the hypothesis of coordinated activation of the C and P circuits in the maintenance of spatial orientation working memory.

Acknowledgements

We thank Dr. Ann-Shyn Chiang's lab for providing several transgenic flies and thank him for his helpful discussion. We also thank Jia-Ying Chien and Tzu-Yu Tseng for acquiring confocal images, and Tzu-Min Wei for the help in the behavioral experiments, and Ta-Shun Su for programming. The work was supported by the Ministry of Science and Technology grants 105-2311-B-007-012-MY3 and 107-2218-E007-033, and by the Higher Education Sprout Project funded by the Ministry of Science and Technology and Ministry of Education in Taiwan.

Author Contributions

RH designed and performed the experiments, analysed the data, wrote the manuscript; H-PH designed the computer models and performed simulations; W-JL designed the computer models; C-LC designed the experiments; H-HY and W-TK designed and constructed the experiment apparatus; H-YC designed the experiments; C-CL designed the study, wrote the manuscript.

Declaration of Interests

The author has no competing financial interests.

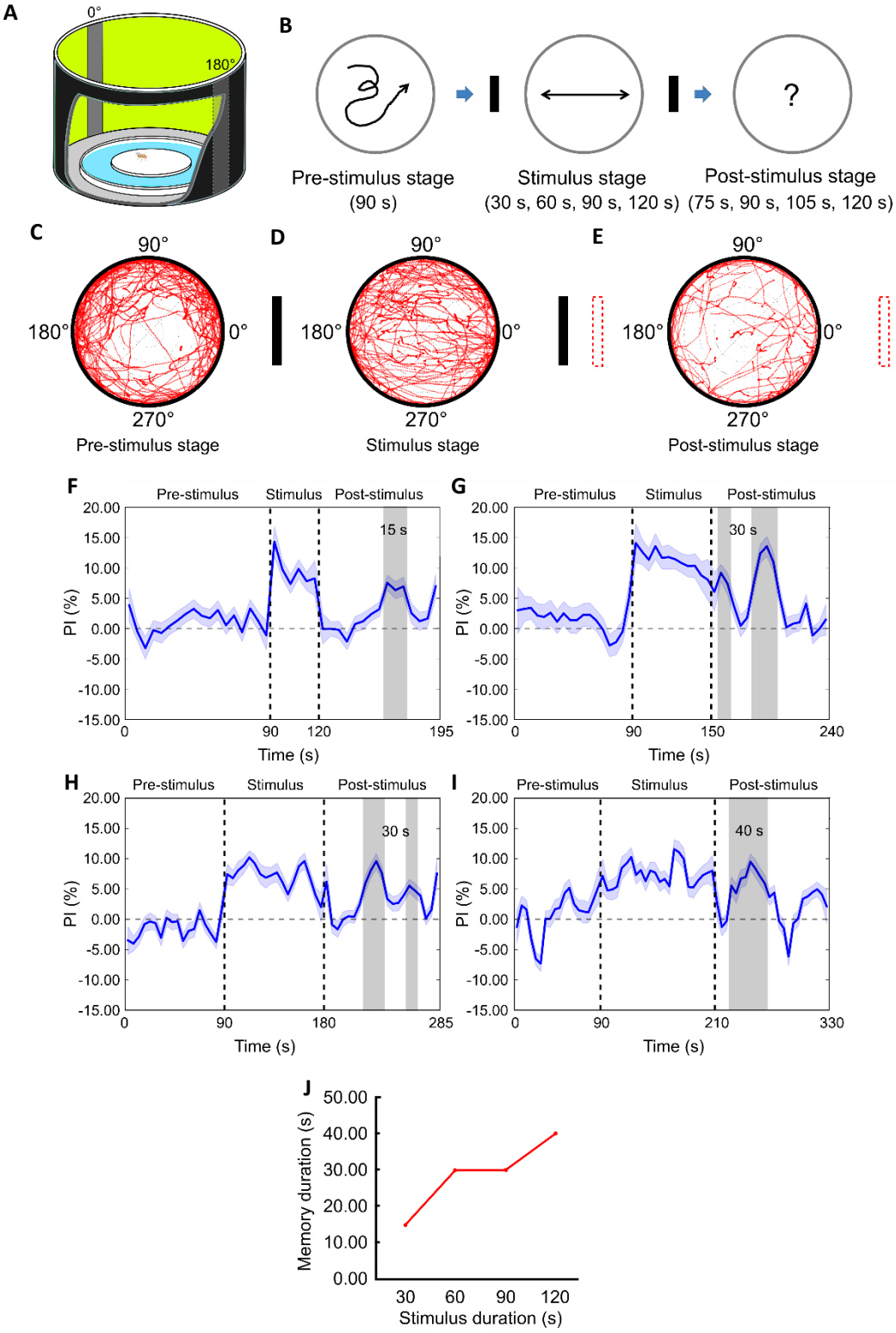

Figure 1. The spatial orientation working memory task for *Drosophila melanogaster* (fruit fly). The performance of the wild-type flies indicated strong working memory of the landmark directions

397 (A) The behavior arena featured a central platform surrounded by water and by a 360°
398 LED screen that displayed two vertical black strips as the visual landmarks at 0° and
399 180°.
400 (B) The task, designed based on Buridan's paradigm [24–26], was divided into three
401 stages: The pre-stimulus stage (90 s), stimulus stage (variable duration), and
402 post-stimulus stage (variable duration). In each trial, a single fruit fly was placed at the
403 center of the platform and was allowed to freely move on the platform in the whole trial.
404 (C-E) The walking patterns as indicated by the red trajectories of the flies (n = 30) in the
405 pre-stimulus, stimulus, and post-stimulus stages. In the stimulus stage, there was a clear
406 pattern of fixation toward the landmarks. The fixation behavior was reduced, but still
407 statistically significant in the post-stimulus stage.
408 (F-I) The performance index (PI) as a function of time with a stimulus stage duration of 30,
409 60, 90, and 120 s, respectively. The shaded regions indicate the periods in which the flies
410 exhibited significant fixation behavior in the post-stimulus stage for 10 s or more.
411 (J) The duration of memory, as indicated by the duration of significant fixation behavior in
412 the post-stimulus stage, was positively correlated with the duration of stimulus stage.

413

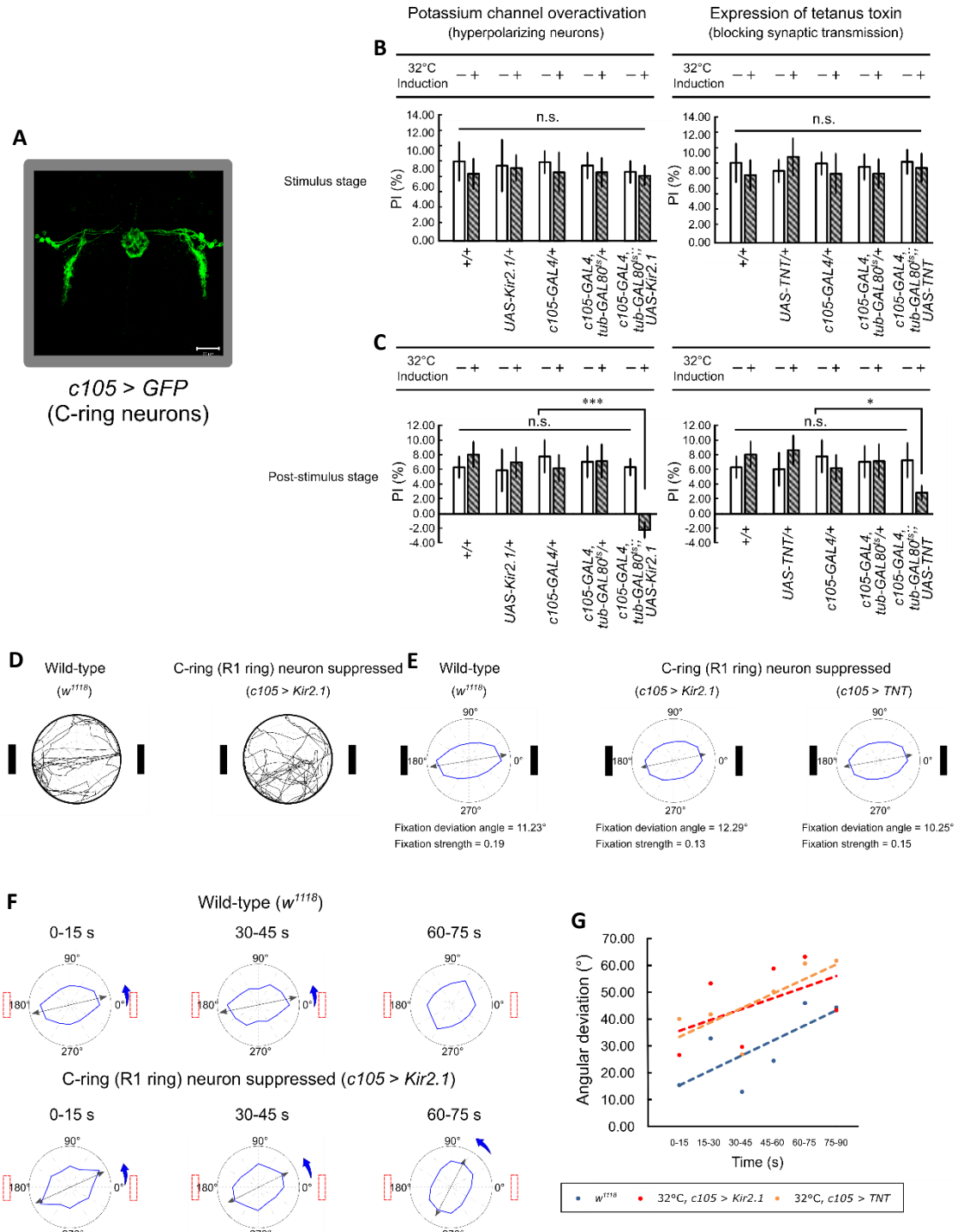

Figure 2. The fruit flies with suppressed C-ring (R1 ring) neurons exhibited reduced fixation behavior and less-accurate orientation memory in the post-stimulus stage

(A) The Gal4 expression domains in the C-ring neurons (*c105-GAL4;; UAS-GFP*).

(B) The performance index (PI) of wild-type flies and flies with suppressed C-ring neurons

420 (left: 32°C, *c105-GAL4, tub-GAL80^{ts};; UAS-Kir2.1*. Right: 32°C, *c105-GAL4, tub-GAL80^{ts};;*
421 *UAS-TNT*) in the stimulus stage. *, **, and *** indicate statistical significance with P-values
422 of < 0.05, < 0.01, and < 0.001, respectively; n.s. = non-significant.
423 (C) Same as in (B), respectively, but for the post-stimulus stage.
424 (D) Sample movement trajectories of a control fly (wild-type, *w^{1118}*) and a fly with
425 suppressed C-ring neurons (32°C, *c105-GAL4, tub-GAL80^{ts};; UAS-Kir2.1*) during the
426 stimulus stage.
427 (E) The radar plots of control flies and flies with suppressed C-ring neurons (both methods)
428 in the stimulus stage indicate that the manipulation of C-ring neurons has a minor effect
429 on fixation behavior.
430 (F) The radar plots of the control group (wild-type: *w^{1118}*) and flies with suppressed C-ring
431 (R1 ring) neurons (32°C, *c105-GAL4, tub-GAL80^{ts};; UAS-TNT*) in different time windows
432 of the post-stimulus stage.
433 (G) Fixation deviation as a function of time for the wild-type files and the two groups
434 submitted to different methods of C-ring neuron suppression during the post-stimulus
435 stage. Dashed lines indicate the linear regression of the color-matched data points. The
436 deviation angle was significantly larger in flies with C-ring neuron suppression than in the
437 wild-type flies.
438

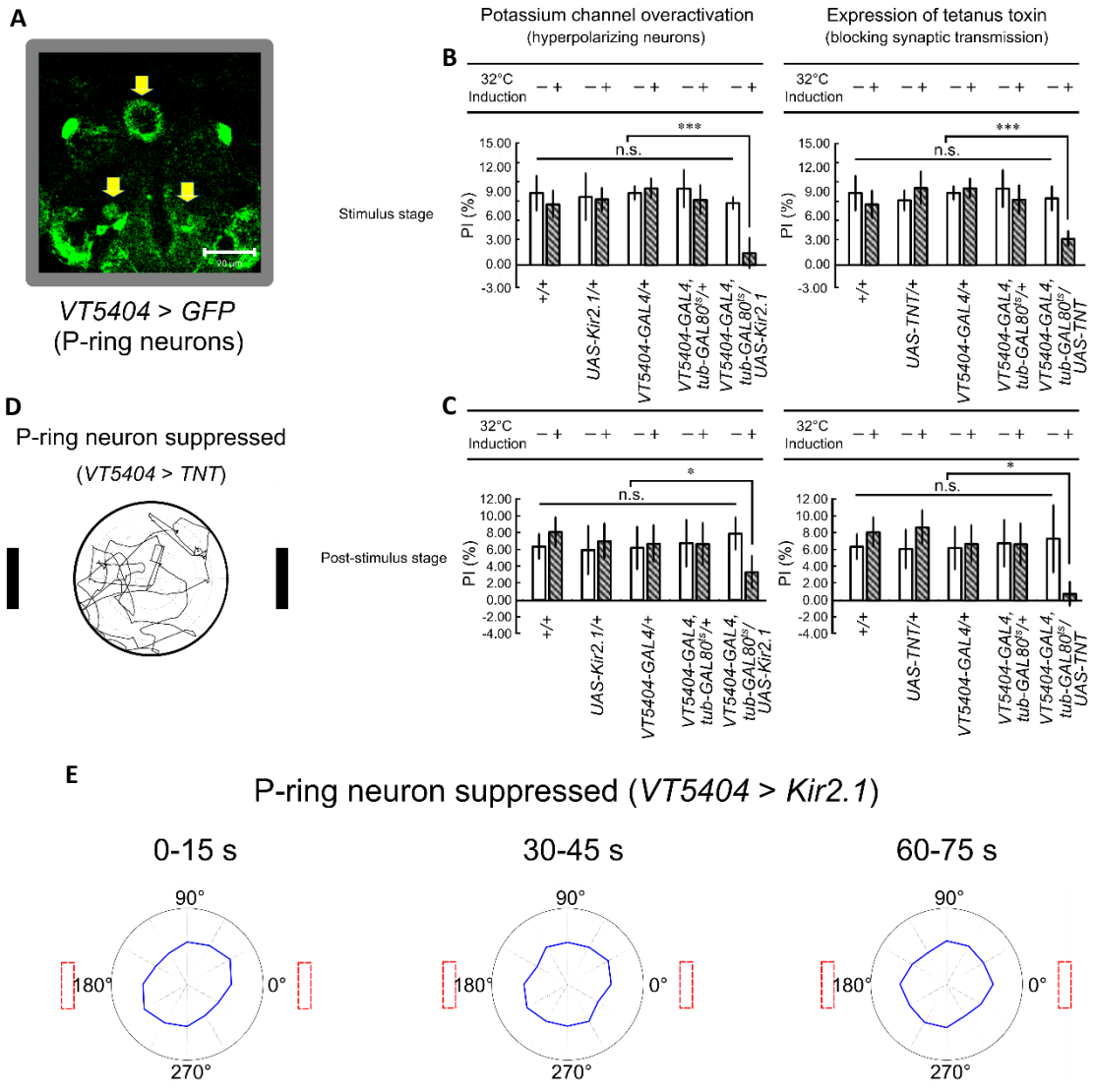

Figure 3. The fruit flies with suppressed P-ring neurons exhibited non-fixation behavior in both stimulus and post-stimulus stages

(A) Gal4 expression domains in the P-ring neurons (*;;VT5404-GAL4/ UAS-GFP*).

(B) The performance index (PI) of the control flies and flies with suppressed P-ring neurons (32°C, *;;VT5404-GAL4, tub-GAL80^{ts}/ UAS-Kir2.1* & 32°C, *;;VT5404-GAL4, tub-GAL80^{ts}/ UAS-TNT*) in the stimulus stage.

(C) Same as in (B), respectively, but for the post-stimulus stage.

(D) Sample movement trajectories of a control fly (wild-type, *w^{1118}*) and a fly with

450 suppressed P-ring neurons (32°C, *;;VT5404-GAL4, tub-GAL80^{ts}/ UAS-Kir2.1*) in the
451 stimulus stage.
452 (E) Radar plots of flies with suppressed P-ring neurons (32°C, *;;VT5404-GAL4,*
453 *tub-GAL80^{ts}/ UAS-TNT*) in different time windows of the post-stimulus stage. *, **, and ***
454 indicate statistical significance with P-values of < 0.05, < 0.01, and < 0.001, respectively;
455 n.s. = non-significant.
456

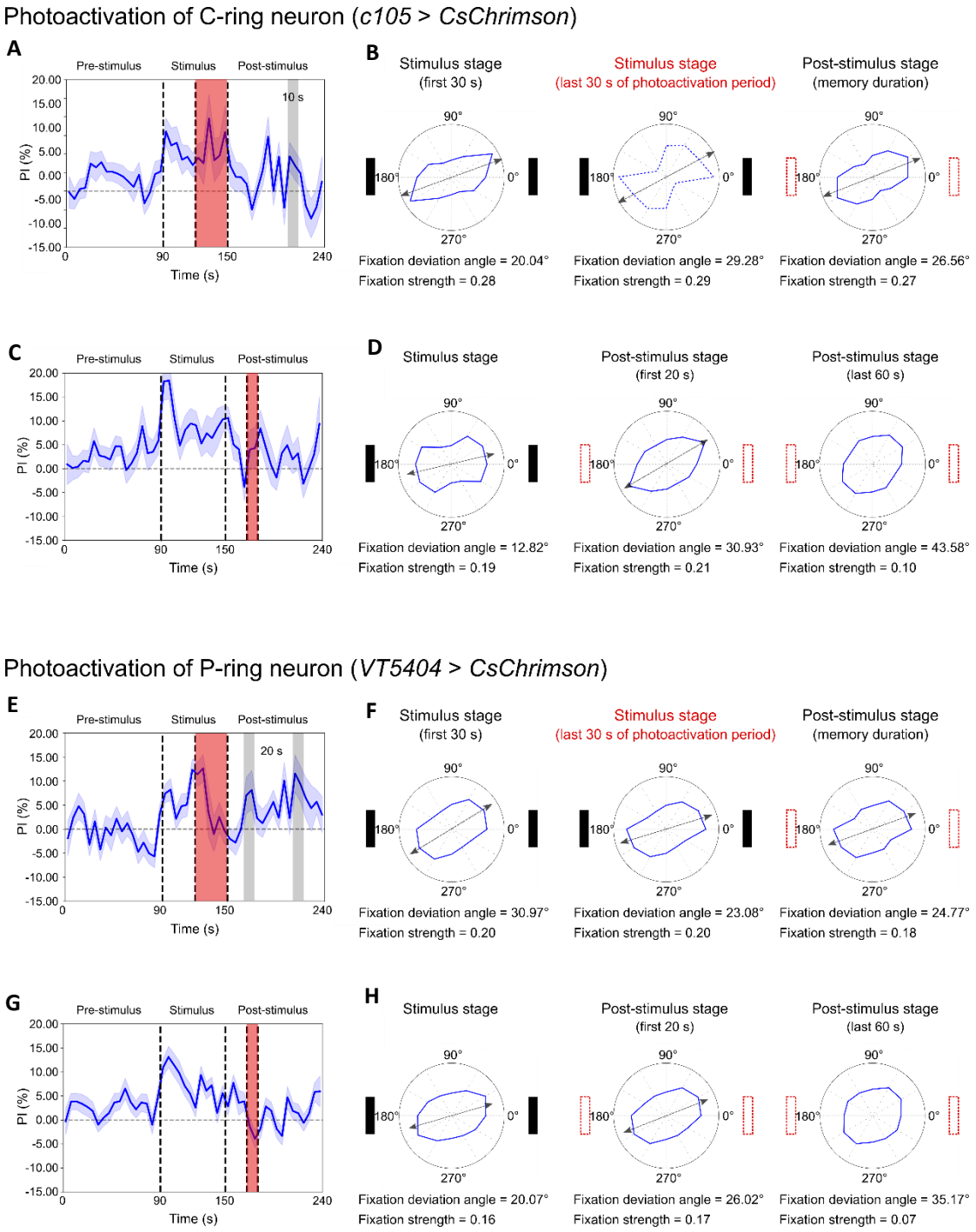

Figure 4. The spatial orientation working memory was abolished when the transient photoactivation of the C-ring or P-ring neurons was applied during the post-stimulus stages. For the transient photoactivation during the stimulus stage, application on the C-ring neurons led to shorter memory duration than on the P-ring neurons

465 (A) The performance index of flies with photoactivation of the C-ring neurons
466 (*c105-GAL4;;UAS-CsChrimson.mVenus*) during the last 30 s of the stimulus stage. The
467 fruit flies exhibited a much shorter fixation behavior (10 s) than the wild-type flies did
468 during the post-stimulus stage.
469 (B) The radar plots for the experiment shown in (A) for the first 30 s of the stimulus stage
470 (left), the last 30 s of the stimulus stage where the photoactivation was applied (middle)
471 and the post-stimulus stage (right). Note that the flies performed very little movement
472 during the period of the photoactivation (Table S3).
473 (C) Same as in (A) but with photoactivation during 20-30 s of the post-stimulus stage. The
474 fixation behavior was abolished after the photoactivation.
475 (D) The radar plots for the experiment shown in (C) for the stimulus stage and the
476 post-stimulus stage before and after the photoactivation.
477 (E-H) Same as in (A-D) but with photoactivation of the P-ring neurons (*;;VT5404-GAL4/*
478 *UAS-CsChrimson.mVenus*). When the photoactivation was applied during the stimulus
479 stage, the fixation behavior during the post-stimulus stage was longer than that with the
480 photoactivation of the C-ring neurons. Additionally, the photoactivation during the
481 post-stimulus stage also abolished the fixation behavior.

482

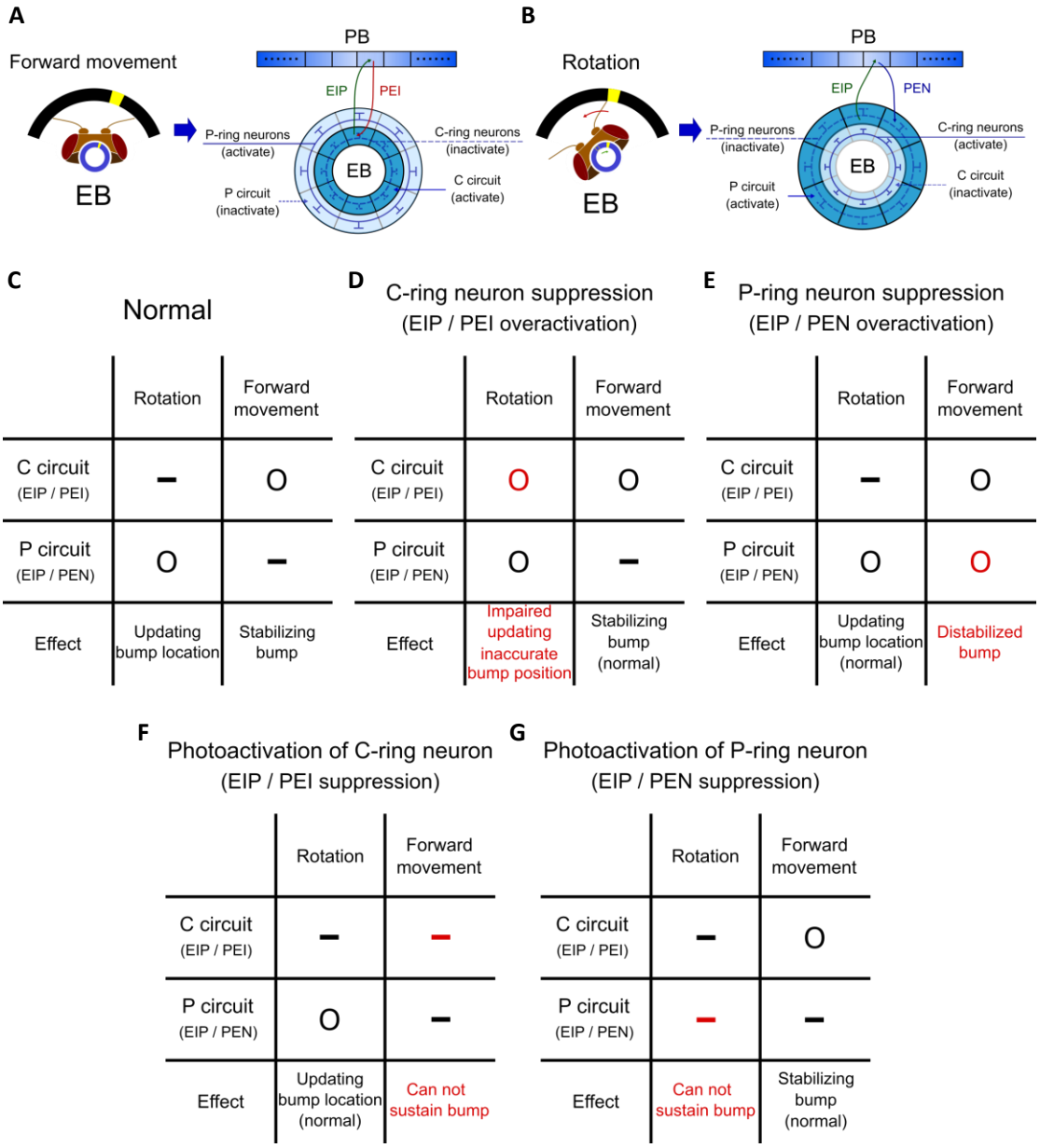

	Rotation	Forward movement
C circuit (EIP / PEI)	–	O
P circuit (EIP / PEN)	O	–
Effect	Updating bump location	Stabilizing bump

	Rotation	Forward movement
C circuit (EIP / PEI)	O	O
P circuit (EIP / PEN)	O	–
Effect	Impaired updating inaccurate bump position	Stabilizing bump (normal)

	Rotation	Forward movement
C circuit (EIP / PEI)	–	O
P circuit (EIP / PEN)	O	O
Effect	Updating bump location (normal)	Distabilized bump

	Rotation	Forward movement
C circuit (EIP / PEI)	–	–
P circuit (EIP / PEN)	O	–
Effect	Updating bump location (normal)	Can not sustain bump

	Rotation	Forward movement
C circuit (EIP / PEI)	–	O
P circuit (EIP / PEN)	–	–
Effect	Can not sustain bump	Stabilizing bump (normal)

Figure 5. The neural mechanisms underlying the behavioral effects of the C-ring or P-ring manipulation can be illustrated by the activation tables based on the hypothesis from a EB-PB circuit model [15]

(A-B) The EB-PB circuit model consists of a symmetric C circuit and an asymmetric P circuit, which are hypothesized to separately activated by forward or rotational movement, respectively. When one circuit is activated, the other is inhibited by the corresponding ring neurons. The C circuit stabilizes the localized neural activity (the bump) that represents

the direction of the landmark, while the P circuit update the bump location when the body rotates.

(C) Based on the model hypothesis, only the C circuit is active during forward movement and only the P circuit is active during rotation movement. The circles and the hyphens indicate activation and inhibition, respectively.

(D) When the C-ring neurons are suppressed, the C circuit becomes continuously activated. The activation over-stabilizes the bump and interferes the updating function of the P circuit during rotation, leading to an inaccurate bump location.

(E) When P-ring neurons are suppressed, the P circuit becomes continuously activated. The overactivation leads to a destabilized bump that diffuses throughout the ring. In such a case, the fly loses its orientation regardless of its movement state.

(F) The photoactivation of the C-ring neurons suppressed the C circuit, causing the loss of the activity bump during the forward movement when the landmark is absent. The loss persists throughout the post-stimulus stage.

(G) The photoactivation of the P-ring neurons produces a similar effect as in (D), but the loss begins during body rotation. Red in panels (D-G) indicates abnormality caused by the ring neuron manipulation.

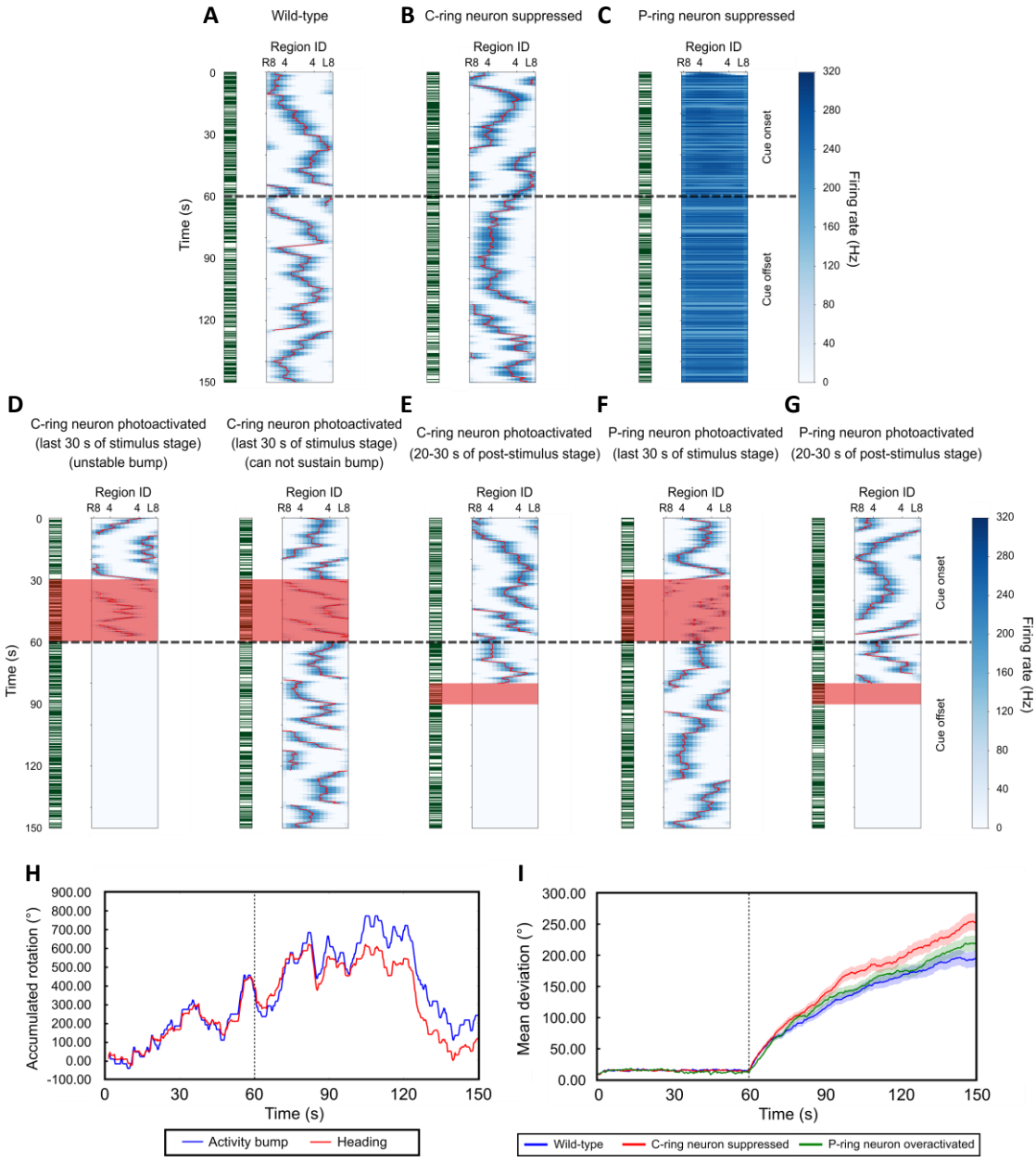

Figure 6. The computer simulations of the EB-PB model [15] **demonstrated the neural mechanisms illustrated in Figure 5, and highlighted the importance of coordinated activation of the C and P circuits in the spatial orientation working memory**

(A) The neural activity of EIP neurons in all EB regions as a function of time indicates the existence of activity bump (dark blue) in a simulated wild-type fly. The landmark was on

between t = 0 s and t = 60 s (dashed line). The green bars on the left indicate the epochs in which the simulated fly performed forward movement.

(B-C) Same as in (A) but with simulated C-ring (B) and P-ring neurons (C) suppression. The P-ring neuron suppression led to unstable and widespread neural activity.

(D-E) Same as in (A), but with simulated photoactivation (red regions) of the C-ring neurons. After the photoactivation in the last 30 s of the stimulus stage (D), the activity bump was disappeared in ~50% of the trials (left) but persisted in the rest trials (right). The photoactivation in the post-stimulus stage always abolished the activity bump (E).

(F-G) Same as in (D) but with the photoactivation of the P-ring neurons in the last 30 s of the stimulus stage (F) or during the post-stimulus stage (G).

(H) The accumulated angles of the true heading and the activity bump of in one sample trial for a simulated wild-type fly.

(I) The trial-averaged angular deviation between the heading and the bump for simulated wild-type flies (blue) and simulated flies with suppressed C-ring neurons (red) or P-ring neuron photoactivation (green). Shades represent the standard error of the mean.

536 **STAR★Methods**

537 **KEY RESOURCES TABLE**

REAGENT or RESOURCE	SOURCE	IDENTIFIE
Experimental Models: Organisms/Strains		
Drosophila melanogaster: w^{1118}	Brain Research Center (BRC)	N/A
Drosophila melanogaster: *;;UAS-Kir2.1*	Brain Research Center (BRC) [35,36]	N/A
Drosophila melanogaster: *;;VT5404-GAL4*	Brain Research Center (BRC)	N/A
Drosophila melanogaster: *;;UAS-CsChrimson. mVenus*	Bloomington *Drosophila* Stock Center (BDSC)	RRID: BDSC_55136
Drosophila melanogaster: *;;UAS-GFP*	Bloomington *Drosophila* Stock Center (BDSC)	RRID: BDSC_1522
Drosophila melanogaster: *tub-GAL80^{ts};;*	Bloomington *Drosophila* Stock Center (BDSC)	RRID: BDSC_7016
Drosophila melanogaster: *;;tub-GAL80^{ts}*	Bloomington *Drosophila* Stock Center (BDSC)	RRID: BDSC_7017
Drosophila melanogaster: *c105-GAL4;;*	Bloomington *Drosophila* Stock Center (BDSC) [29]	RRID: BDSC_30822
Drosophila melanogaster: *;;UAS-TNT*	Bloomington *Drosophila* Stock Center (BDSC) [37,38]	RRID: BDSC_28997

Drosophila melanogaster: *;;ninaE*	*Drosophila* Genomics Resources Center (DGRC)	RRID: DGRC_109599
Software and Algorithms		
Arduino Shield MEGA2560	https://www.arduino.cc/	N/A
RED LED SMD 5050	https://www.sunrom.com/p/red-led-smd-5050	N/A
Zeiss LSM 510	https://www.zeiss.com/corporate/int/home.html	N/A
Statistical Product and Service Solutions 22.0 (SPSS 22.0)	https://www.ibm.com/analytics/spss-statistics-software	N/A
Python 3.7	https://www.python.org/	N/A
Fiji (ImageJ)	NIH	N/A

538

539 **LEAD CONTACT AND MATERIALS AVAILABILITY**

540 Further information and requests for resources and reagents should be directed to and will
541 be fulfilled by the Lead Contact, Chung-Chuan Lo (cclo@mx.nthu.edu.tw). Fly stocks
542 generated in this study are available at Nation Tsing Hua University.

543

544 **EXPERIMENTAL MODEL AND SUBJECT DETAILS**

545 Flies were raised at 25°C with a 12:12 h light-dark cycle with a humidity level of ~50%.
546 Wild-type and transgenic flies were obtained from the Bloomington *Drosophila* Stock
547 Center, *Drosophila* Genomics Resources Center and Brain Research Center (BRC) in
548 National Tsing Hua University (NTHU) (see Key Resources Table for detail). For the
549 neuron suppression experiments, all Gal4 lines were crossed to the *UAS-Kir2.1* or
550 *UAS-TNT* effector lines and the expression can be controlled by temperature with the
551 combination of *tub-GAL80*^{ts}. For the optogenetic experiments, all Gal4 lines were crossed
552 to the *UAS-CsChrimson.mVenus* effector lines.

553

554 **METHOD DETAILS**

555 **The arena**

556 We conducted the behavioral tasks with flies in a circular arena constructed in house. We
557 followed the general design principles described in previous studies [10]. The arena had a
558 central circular platform of 85 mm in diameter and was surrounded by a 360° LED display
559 with water filling the basin surrounding the platform (Figure 1A). The display was made of
560 38 LED panels and each panel consists of five matrices of 8 × 5 LEDs. The entire LED
561 screen measured 260 mm in diameter and 190 mm in height. We used green LEDs with a
562 wavelength of 572 nm, which is close to the peak sensitivity of a fly's vision [39]. Each
563 vertical line of the LEDs could be individually controlled by a personal computer via an
564 Arduino board (Arduino Shield MEGA2560). A CCD camera was mounted directly above
565 the platform and was used to record the movement trajectories of the flies using a Python
566 script developed in house.

567

568 **The spatial orientation memory task**

569 We used 3-5 day-old flies and clipped the wings 1 day before the experiments [25]. In
570 addition to wild-type flies (genotype: w^{1118}), we used flies with suppressed C-ring or P-ring
571 neurons, which was achieved by hyperpolarizing the neurons (32°C, *c105-GAL4,*
572 *tub-GAL80^{ts};; UAS-Kir2.1* for C-ring neuron suppression and *;;VT5404-GAL4, tub-GAL80^{ts}*
573 */ UAS-Kir2.1* for P-ring neuron suppression) or by blocking the neurotransmitters (32°C,
574 *c105-GAL4, tub-GAL80^{ts};; UAS-TNT* for C-ring neuron suppression and *;;VT5404-GAL4,*
575 *tub-GAL80^{ts} / UAS-TNT* for P-ring neuron suppression). After the wings were clipped, the
576 flies were placed in an 18°C incubator for cold-shock or in a 32°C incubator for heat-shock
577 for 1 day. All experiments were performed between 10am and 5pm. We also used
578 optogenetics to transiently activated C-ring or P-ring neurons. The expression of the
579 effector (*UAS-CsChrimson.mVenus*) was controlled by red lights (625 nm) exposure after
580 feeding all-*trans*-retinal (100 μM) in a dark environment for 7 days [40].

581 The spatial orientation memory task consisted of three stages: The pre-stimulus
582 stage, stimulus stage, and post-stimulus stage (Figure 1B). Only one fly was submitted to

583 the task in each trial and the fly was allowed to freely move on the circular platform. The
584 pre-stimulus stage lasted 90 s, during which all LEDs were turned on and no visual
585 landmark was presented on the screen. During the stimulus stage, two vertical black strips,
586 each 30° wide and separated by 180°, were presented on the screen as visual landmarks
587 (Figure S1D). We tested four different durations (30, 60, 90 and 120 s) for the stimulus
588 stage with wild-type flies, and used 60 s in the subsequent neural functional experiments.
589 In the post-stimulus stage, the two landmarks were removed and all LEDs were turned on;
590 this stimulus condition was identical to that used in the pre-stimulus stage. The duration of
591 the post-stimulus stage was 75, 90, 105, and 120 s for the four different durations of 30,
592 60, 90, and 120 s of the stimulus stage, respectively. The movement trajectories of the
593 flies were recorded using a CCD camera at a speed of 20-25 frames per second. The
594 position of the fly in each frame was captured by a Python script and saved for
595 post-experiment analysis.
596
597 **Optogenetic activation**
598 Red LED array made up of 96 LEDs (625 nm, RED LED SMD 5050, 20 mW/mm^2) were
599 used to activate *CsChrimson* during the behavioral task. The LED array was placed below
600 the platform in the arena. The platform was made of acrylonitrile-butadiene-styrene (ABS)
601 and was partially transparent to light due to its 1mm of thickness. We used two protocols
602 of photo activation. In the first protocol, the red light was turned on during the last 30 s of
603 the stimulus stage. In the second protocol, the red light was turned on for only 10 s
604 starting at 20 s after the post-stimulus stage began.
605
606 **The EB-PB model**
607 We used a previously proposed partial central complex model [15], which was built based
608 on the connectomic data of the EB and PB [6,30]. The model was simulated using the
609 Flysim simulator [43]. The model network consists of two coupled ring circuits: One with
610 symmetric recurrent excitatory connections (C circuit) formed by EIP (or E-PG) and PEI
611 neurons and one with asymmetric excitatory connections (P circuit) formed by EIP and

612 PEN (or P-EN) neurons [16,20,21] (Figures 6A and 6B). Each of the rings is mapped
613 topographically to 360° of the horizontal plan of the external space. The C circuit is able
614 to form a stable and localized activity (the activity bump), which corresponds to the
615 orientation of a salient object. The P circuit moves the activity bump in the clockwise or
616 counterclockwise direction on the EB based on the unilateral input to PB. This unilateral
617 input carries the self-motion cue about the rotational speed of the body, and is presumably
618 originated from the motor feedback or from the acceleration sensing organs. The P-ring
619 function is required when a fruit fly rotates its body because the bump must move in the
620 counter-direction in order to compensate for the body rotation. Such counter movement
621 allows the activity bump to remain in the EB subregions that correspond to the direction of
622 a fixed reference point in space.
623
624 **The control of behavior in the model**
625 The main goal of the model was to demonstrate whether the EB-PB circuits are capable of
626 maintaining and updating the activity bump under the given experimental conditions so
627 that an accurate orientation is available to the flies when they want to fixate on the
628 landmarks. We did not ask and modelled when the flies decide to fixate and how do they
629 move their bodies for this purpose. These behavioral controls are likely to be carried out in
630 other brain regions and are out of the scope of the present study. Therefore, here we
631 model the behavior of the fly using a random movement protocol, which consists of two
632 movement states, forward movement and rotation. The model switch between the two
633 states randomly based on the Markov chain dynamics (see the section "The model
634 parameters" below). In the model, a movement state lasted for a minimum length of one
635 time step (300 ms). At the end of each time step, the fly switches to the other state or
636 remains in the same state based on preset probabilities that are independent of the history.
637 The probability of switching from forward movement to rotation is 0.40 and from rotation to
638 forward movement is 0.60. These numbers were derived by analysing the distribution of
639 bout length for each movement type in the behavioral tasks (see "The model parameters"
640 section below).

641 During the forward movement state, the fly maintains its orientation without turning,
642 while during the rotation state, the fly rotates in a randomly selected direction until the end
643 of the state. The body rotation is modelled by applying input to the unilateral PB [15].
644
645 **The simulated behavioral task**
646 We simulated the second (stimulus) and the third (post-stimulus) stages of the behavioral
647 task. In the simulation, the two stages are represented by landmark onset and offset,
648 respectively. In the stimulus stage, the model received visual input from the landmark and
649 the signal about the movement state (forward or rotation) from the behavioral control
650 module described above. The visual input was modelled by sending spike input to the PB
651 subregions which trigger an activity bump in the EB that corresponds to the landmark
652 location. For the forward movement state, the P-ring neurons were activated to suppress
653 the P circuit and the C circuit were allowed to operate in order to stabilize the activity
654 bump in a specific location. For the rotation state, the C-ring neurons were activated for
655 suppressing the C circuit. At the same time, an input to all subregions in the unilateral PB
656 was applied in order to shift the activity bump in the P circuit. Input to the left side of the
657 PB induced clockwise rotation of the activity bump, while input to the right side of the PB
658 induced counterclockwise rotation. This movement feedback is used to model the
659 observed counter-movement of the activity bump when the fly rotates its body. In the
660 post-stimulus stage, the visual input was turned off, while the movement signal remained.
661 Approximately 200 trials were simulated for each experimental condition.
662
663 **The model parameters**
664 The parameters of the EB-PB model mainly follow those used in a previous study [15], but
665 some parameters were modified in this study (Table S4). The parameters of the
666 behavioral model were determined by the behavioral experiment described in this study.
667 We analysed the movement patterns of the flies during the first (pre-stimulus) stage and
668 used them to determine the parameters associated with the forward movement and
669 rotation state. By fitting an exponential curve to the distribution of the forward movement

670 bouts, and the body rotation bouts (Figures. S6A and S6B), we can determine the
671 probabilities that a fly switch between the forward movement states and the rotation state.
672 Based on the result, we constructed a Markov chain model of the random walk behavior of
673 the fruit flies (Figure S6C).

674 There was one additional pair of parameters to be determined: The activation level of
675 the C-ring and P-ring neurons in the ring-neuron suppression and photoactivation
676 experiments. We left these as the free parameters and determined them by matching the
677 radar plots of the simulated behavior to those of the actual ring-neuron suppression
678 experiments. For the wild-type fly simulation, the spike rate of input to C-ring and P-ring
679 neurons was 150 Hz. For the simulated flies with suppressed C-ring neurons, the input
680 was reduced to 75 Hz, while for the simulated flies with suppressed P-ring neurons, the
681 input was reduced to 50 Hz. For photoactviation of C-ring and P-ring neurons, the input
682 spike rates were 100Hz.

683

684 **QUANTIFICATION AND STATISTICAL ANALYSIS**

685 **Confocal images**

686 7-day-old adult flies brains were fixed, mounted in phosphate buffer saline (PBS) as
687 previously described [41]. Images were scanned with Zeiss LSM 510 confocal
688 microscopy.

689

690 **Data analysis**

691 To analyse the movement direction of each fly [42] in each video frame, we first calculated
692 the speed vector based on the difference in the coordinates of the fly between two
693 consecutive frames. The movement direction was represented by the degree value on the
694 screen at the point that the speed vector projected to (Figure S1A). For better presentation
695 and analysis, we calculated the summed percentages, $p(\theta)$, of the movement direction in
696 each of the 12 quantiles in 360°. θ represents the center degree of the quantile. Each
697 quantile spans 30° on the screen. Fixation behavior was characterized by a significantly
698 higher percentage of the movement direction falling within $\pm$15° of 0° and 180° on the

screen, the quantiles that the two visual landmarks occupied. We pooled the data in 5 s or 15 s time bins, depending on the purpose of the analysis.

We determined the behavioral performance of the flies by calculating the performance index (PI) and by plotting the radar plots. The PI was calculated by subtracting the percentage of movement direction in the quantiles centered at 90° and -90° from that in the quantiles centered at 0° and 180° (the landmark quantiles):

$$PI = p(0°) + p(180°) - p(90°) - p(-90°). \quad (1)$$

The index indicates the difference between the frequencies of movement toward the visual landmarks and toward the perpendicular directions. A high index indicates a strong tendency of fixation behavior toward the visual landmarks, while a low index indicates either non-fixation behavior or fixation behavior toward a direction that is different from the landmarks.

To quantify the duration of spatial orientation working memory in the post-stimulus stage, the memory is defined to be present in an interval if the population-averaged PI is significantly larger than zero for 10 s (two time bins) or more, and the PI is higher than that in pre-stimulus stage.

To investigate whether the fixation direction had shifted from the landmark position, we calculated the $PI_{\text{landmark-adjacent}}$, which is defined as the frequency of movement direction in the landmark quantiles minus 50% of those in in the adjacent quantiles (centered at 30, 150, 210, and 330°):

$$PI_{\text{landmark-adjacent}} = p(0°) + p(180°) - (p(30°) + p(-150°) + p(-30°) + p(150°))/2. \quad (2)$$

A more detailed indication of the fixation behavior can be obtained from the radar plot, which indicates the frequencies of the movement direction in each quantile. In the plot, each pair of quantiles that are 180° apart, e.g. quantiles centered at 90° and -90°, is represented by the same value, which is their averaged percentage. This makes the radar plot point-asymmetric. If a fly did not exhibit any fixation behavior, it would move toward any direction with equal probability due to the point symmetric property of the arena, and the expected value of each pair of quantiles on the plot is 1/6 (~16.67%). A value that is significantly different from 1/6 indicates some form of fixation behavior.

The radar plots allow us to visually inspect the existence of fixation behavior and the main direction that the flies fixated on with respect to the directions of the visual landmarks. To further quantify these two behavioral properties, we calculated the fixation deviation angle (σ_f) and the fixation strength (F). The fixation deviation angle (σ_f) represents the direction of the strongest fixation tendency and is defined by the angle σ, which yields the smallest second moments $M(\sigma)$ on the radar plot:

$$M(\sigma_f) \equiv \min_{\sigma}\left(\sum_i p(\theta_i)^2 \sin^2(\theta_i - \sigma)\right), \tag{3}$$

where θ_i is the angle of each quantile (0°, 30°, 60°, 90°, ….). σ_f can be obtained by taking the derivative of $M(\sigma)$ with respect to σ.

$$\left.\frac{dM(\sigma)}{d\sigma}\right|_{\sigma=\sigma_f} = 0. \tag{4}$$

Plugging θ_i and $p(\theta_i)$ into this equation and solving for σ using trigonometric identities, we obtain

$$\sin(2\sigma_f + \phi) = 0 \tag{5}$$

and

$$\sigma_f = \frac{-\phi}{2} \text{ or } \sigma_f = \frac{180-\phi}{2} \tag{6}$$

where ϕ is a variable depending on $p(\theta_i)$ based on the following equations:

$$\cos\phi = A/K \text{ and } \sin\phi = B/K \tag{7}$$

$$A = 2p(0°)^2 + p(30°)^2 - p(60°)^2 - 2p(90°)^2 + p(-30°)^2 - p(-60°)^2 \tag{8}$$

$$B = \sqrt{3}(p(-30°)^2 - p(30°)^2 + p(-60°)^2 - p(60°)^2) \tag{9}$$

$$K = \sqrt{A^2 + B^2}. \tag{10}$$

The deviation angle given in Equation (6) corresponds to two values. One gives rise to the minimum value of M (denoted as $M_{\min}$) and the other gives rise to the maximum value of M (denoted as $M_{\max}$). Finally, the fixation strength (F) is defined as follows:

$$F = 1 - \frac{M_{\min}}{M_{\max}}. \tag{11}$$

Analysis of locomotion

To test whether the genetic manipulation in the central complex led to a deficit in

755 locomotion, which in turn contributed to the change in fixation behavior, we analysed the
756 average movement speed and activity level of the flies. The average speed was
757 calculated by dividing the total movement distance by the total duration of movement in
758 one stage of the task. The activity level was defined as the percentage of video frames in
759 which the fly moved.
760
761 **Vision test**
762 We tested the vision of the flies to ensure that the observed behavioral changes were not
763 due to vision impairment. In the first stage of the test, we allowed a fly to freely move on
764 the platform for 60 s. In the second stage, we put a laser spot (50 mW, wavelength = 532
765 nm) on the platform and gradually moved the spot toward the fly until the laser hit the fly's
766 body. We repeated this procedure several times. Due to its power, the laser spot is
767 strongly aversive to the flies, and they quickly learned to avoid the laser spot. Typically,
768 after a couple of hits, the flies began to escape the approaching laser spot before it
769 reached them. As a control, we also tested flies with deficient photosensors
770 (genotype: *;;ninaE*) (Video S1). Such escape behavior would not occur if the flies could
771 not visually perceive the approaching laser spot. We measure the escape rate, r, which is
772 defined as:
773 $$r = \frac{\text{Number of escapes}}{\text{Total number of laser approaching events}}. \quad (12)$$
774 We then compared r between the transgenic flies and the wild-type flies. We would
775 expect a lower r for the flies if they were visually impaired.
776
777 **Statistical analysis**
778 For wild-type flies, 10-25 individuals were used for each experimental condition in the
779 short-term orientation memory test. For the neural functional experiments and optogenetic
780 activation experiments, 10-20 flies were used in each group.
781 The statistical analyses were performed using Statistical Product and Service
782 Solutions 22.0 (SPSS 22.0). A multi-factor within group analysis of variance was used to
783 analyse the performance index, and a mixed variance analysis was used to evaluate

differences between groups with different genetic conditions.

DATA AND CODE AVAILABILITY

The data and code used in this study are available upon request to the corresponding author.

790 **Supplemental Information**

791 **Table S1. Fixation deviation and fixation strength of wild-type *Drosophila* in the**

792 **post-stimulus stage before and during the fixation period**

793

Period	Measure of memory quality	Stimulus stage duration (s)			
		30	60	90	120
Pre-fixation	Fixation deviation angle(°)	2.11	12.35	8.56	50.54
	Fixation strength	0.02	0.09	0.03	0.04
Fixation	Fixation deviation angle(°)	10.16	0.75	1.98	3.00
	Fixation strength	0.11	0.18	0.14	0.11

794

795 **Table S2. Fixation deviation and fixation strength of wild-type flies, flies with suppressed C-ring neurons, and flies with suppressed P-ring**

796 **neurons in different time windows of the post-stimulus stage**

797

Type of fly	Genotype	Measure of fixation behavior	Time in the post-stimulus stage (s)							
			0-15	15-30	30-45	45-60	60-75	75-90	15-45	45-75
Wild-type	w^{1118}	Fixation deviation angle(°)	15.26	32.64	12.74	24.32	45.79	44.15	15.29	30.25
		Fixation strength	0.15	0.11	0.17	0.12	0.08	0.07	0.11	0.09
Suppression of C-ring neurons	32°C, *c105-GAL4, tub-GAL80^{ts};;UAS-Kir2.1*	Fixation deviation angle(°)	26.43	53.17	29.50	58.65	63.06	43.16	38.38	63.51
		Fixation strength	0.16	0.07	0.12	0.12	0.13	0.12	0.07	0.11
	32°C, *c105-GAL4, tub-GAL80^{ts};;UAS-TNT*	Fixation deviation angle(°)	39.88	41.60	26.66	50.10	60.53	61.57	31.61	58.75
		Fixation strength	0.11	0.07	0.13	0.11	0.13	0.11	0.10	0.10
Suppression of P-ring neurons	32°C, *;;VT5404-GAL4, tub-GAL80^{ts}/ UAS-Kir2.1*	Fixation deviation angle(°)	37.78	38.69	49.81	32.36	36.77	43.06	43.98	29.97
		Fixation strength	0.10	0.06	0.08	0.05	0.07	0.05	0.05	0.05
	32°C, *;;VT5404-GAL4, tub-GAL80^{ts}/ UAS-TNT*	Fixation deviation angle(°)	35.17	46.36	37.77	53.19	51.40	45.52	52.55	55.23
		Fixation strength	0.10	0.10	0.08	0.10	0.08	0.10	0.04	0.06

798 **Table S3. Activity level and movement speed of wild-type flies, flies with**
799 **suppressed C-ring or P-ring neurons and flies with photoactivated C-ring or P-ring**
800 **neurons.**
801

Wild-type and neural deficits	Genotype	Activity level (%)	Speed (mm/s)
Wild-type	*w*^{1118}	88.05 ± 1.04	9.86 ± 0.43
Suppression of C-ring neurons	32°C, *c105-GAL4, tub-GAL80*^{ts}*;;UAS-Kir2.1*	81.50 ± 0.54	8.97 ± 0.24
	32°C, *c105-GAL4, tub-GAL80*^{ts}*;;UAS-TNT*	82.30 ± 0.78	8.57 ± 0.41
Suppression of P-ring neurons	32°C, *;;VT5404-GAL4, tub-GAL80*^{ts}*/ UAS-Kir2.1*	83.01 ± 0.98	8.47 ± 0.49
	32°C, *;;VT5404-GAL4, tub-GAL80*^{ts}*/ UAS-TNT*	86.44 ± 1.55	11.26 ± 1.37
Photoactivation of C-ring neurons	*c105-GAL4;; UAS-CsChrimson.mVenus*	33.74 ± 7.09	6.20 ± 0.69
Photoactivation of P-ring neurons	*;;VT5404-GAL4, tub-GAL80*^{ts}*/ UAS-CsChrimson.mVenus*	79.71 ± 3.02	12.05 ± 0.90

802
803

Table S4. Synaptic weights between neuron types

Source	Destination			
	EIP	PEI	PEN	Ring-EIP
EIP		4.0	4.0	1.0
PEI	8.0/4.0/4.0*			
PEN	10.0/5.0/15.0**			
Ring - EIP	3.0			1.6
Ring - PEI		10.0		
Ring - PEN			10.0	

* The first and second numbers indicate the synaptic weights of the central connections, e.g. PEI0→EIP10, and the peripheral connections, e.g. PEI0→EIP2. The third number indicates the atypical connections, e.g. PEI7 / PEI8 → EIP0 / EIP17.

** The first and second numbers indicate the synaptic weights of the central connections, e.g. PEN0→EIP10, and the peripheral connections, e.g. PEN0→EIP2. The third number indicates the atypical connections, e.g. PEN7 / PEN8 → EIP0 / EIP17.

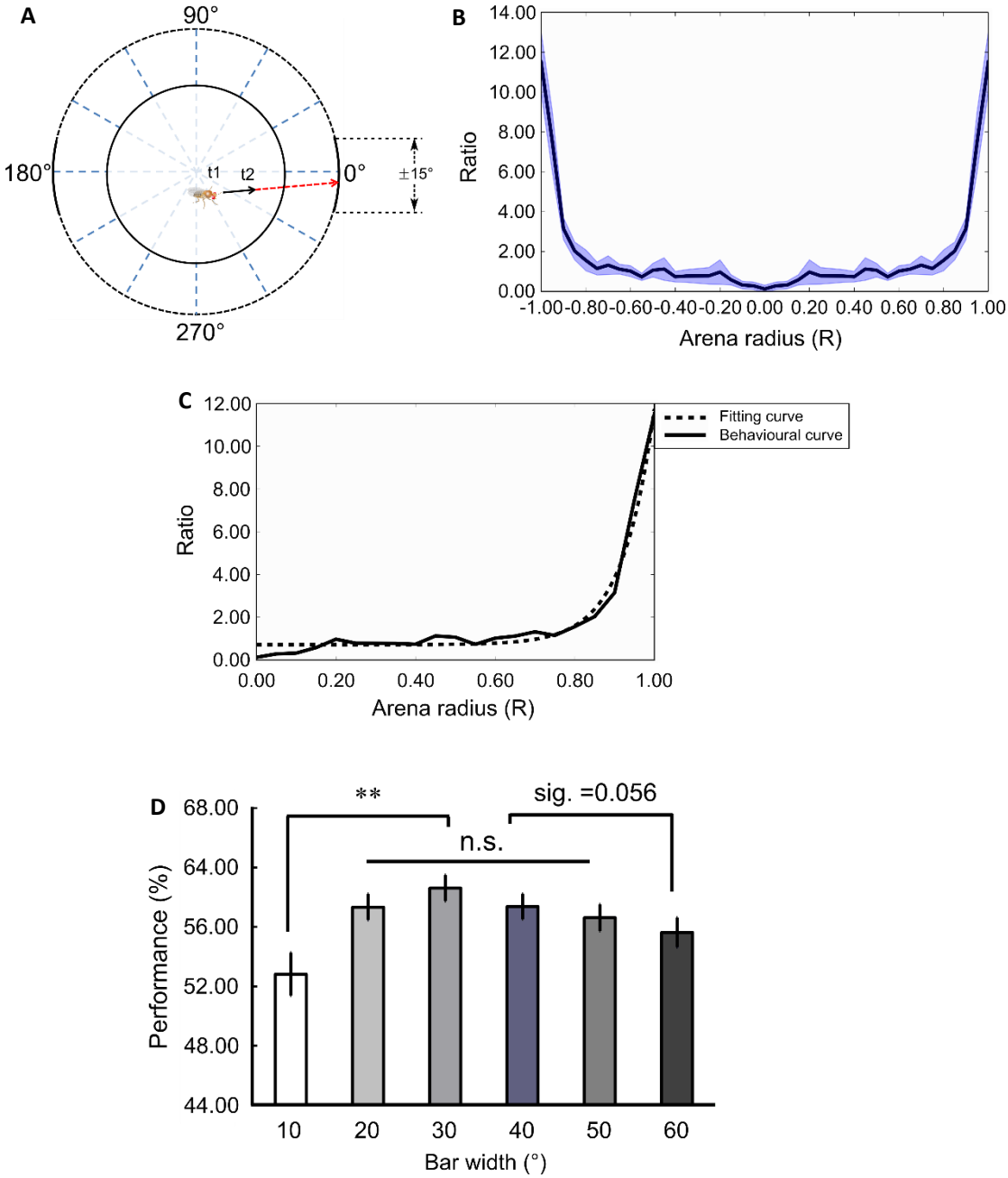

Supplementary Figure S1. Measurements and statistics of fruit fly movements in the task

(A) In the behavioral task, we recorded the heading direction of the fly in each time step by calculating the vector (black arrow) that connects the positions of the fly in the previous (t1) and present (t2) time steps. The heading direction is defined by the projection (red arrow)

of the vector on the LED screen. The heading direction is 356° (or -4°) in this case.

(B) The distribution of the position of flies on the platform along the radius during the pre-stimulus stage. The shaded area indicates the standard error of the mean. The values were normalized by the area spanned in each unit length of the radius.

(C) The curve presented in (B) can be fitted by an exponential function, $y = ae^{bx} + c$, where $a = 3.7 \times 10^{-5}$, $b = 12.594$, $c = 0.715$. The coefficient of determination, $R^2 = 0.983$.

(D) The performance of visual fixation depends on the width of the visual landmarks. We tested the performance (normalized by the landmark width) of the flies against different landmark widths and found that the best performance fell within the range of 20-40°. Based on this result, we set the landmark width to 30° in the present study. n.s. = non-significant.

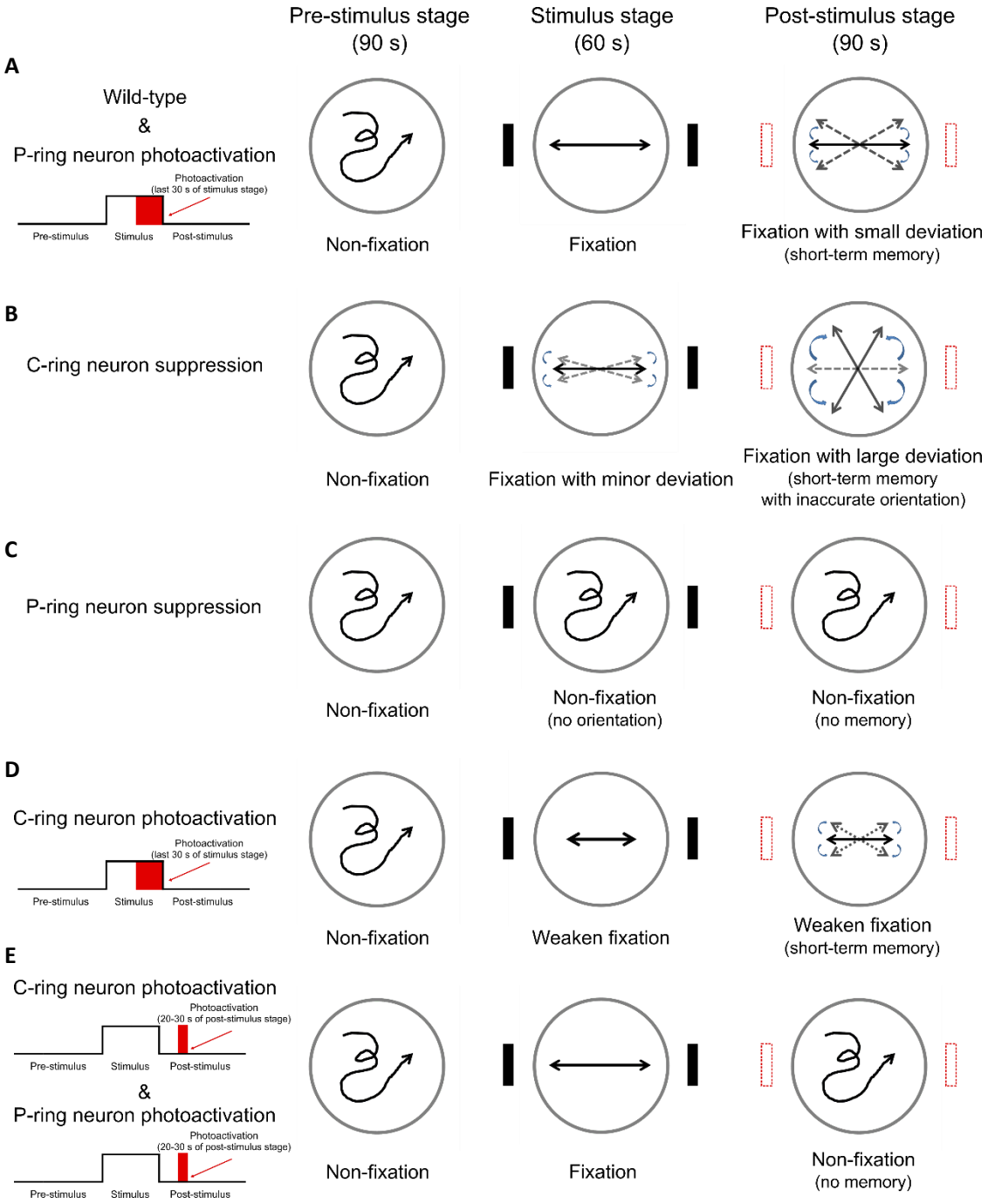

Supplementary Figure S2. Schematic that summarizes the behavioral effects of C-ring and P-ring neuron suppression and photoactivation

(A) Wild-type flies maintain fixation behavior in both the stimulus stage and the post-stimulus stage, in which the flies exhibited a slight deviation in the fixation direction.

842 Flies with transient photoactivation of the P-ring neurons during the stimulus stage
843 exhibited a similar behavioral pattern.
844 (B) Flies with suppressed C-ring neurons exhibited fixation behavior with small and large
845 deviations in the stimulus and post-stimulus stages, respectively.
846 (C) Flies with suppressed P-ring neurons could not maintain fixation behavior, indicating
847 loss of spatial orientation.
848 (D) Flies with photoactivation of the C-ring neurons during the last half of the stimulus
849 stage strongly reduced the fixation behavior during the post-stimulus stage.
850 (E) Flies with transient photoactivation of the C-ring or P-ring neurons during the early
851 post-stimulus stage eliminated the fixation behavior.
852

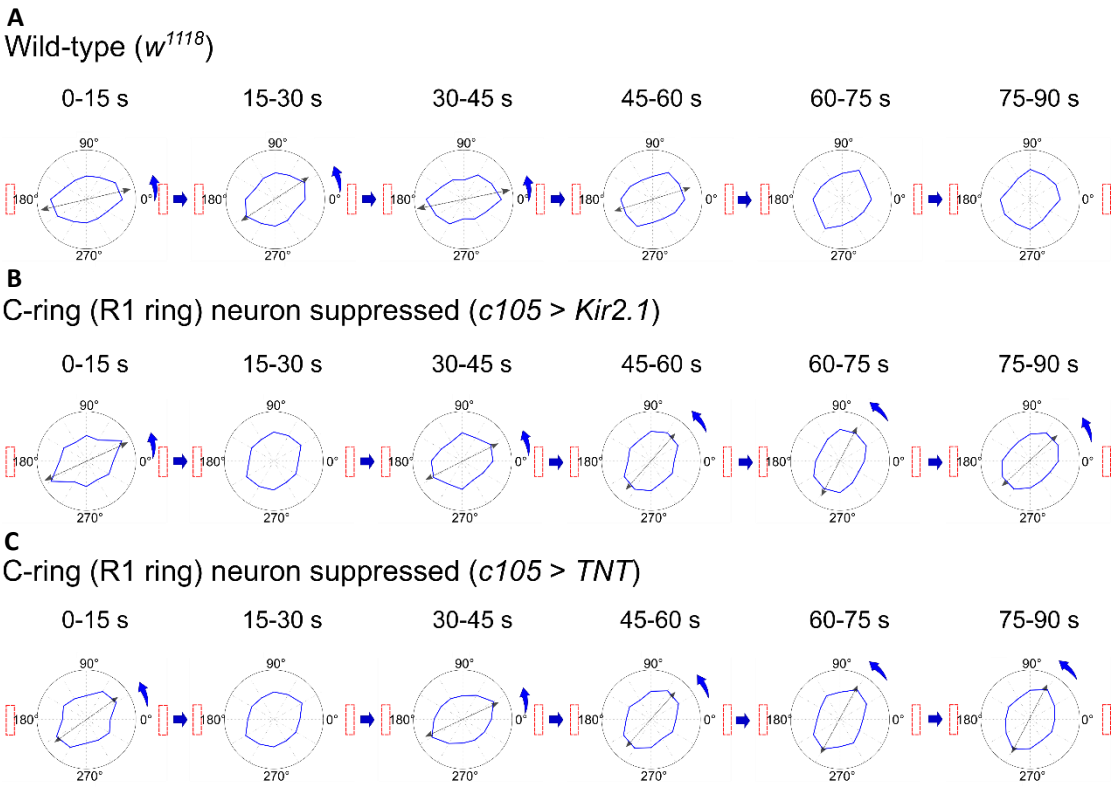

Supplementary Figure S3. Radar plots of the flies in the control groups (wild-type: *w*^{1118}) and flies with suppressed C-ring (R1 ring) neurons

(A) Wild-type *Drosophila* (genotype: *w*^{1118}).

(B-C) Flies with suppressed C-ring neurons ((B) for 32°C, *c105-GAL4, tub-GAL80*^{ts}*;; UAS-Kir2.1* and (C) for 32°C, *c105-GAL4, tub-GAL80*^{ts}*;; UAS-TNT*) in the post-stimulus stage.

863 **A**
P-ring neuron suppressed (*VT5404* > *Kir2.1*)

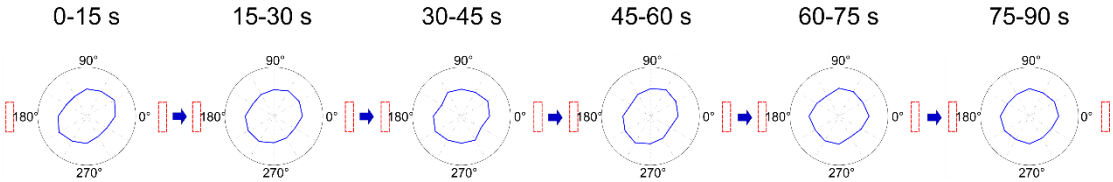

B
P-ring neuron suppressed (*VT5404* > *TNT*)

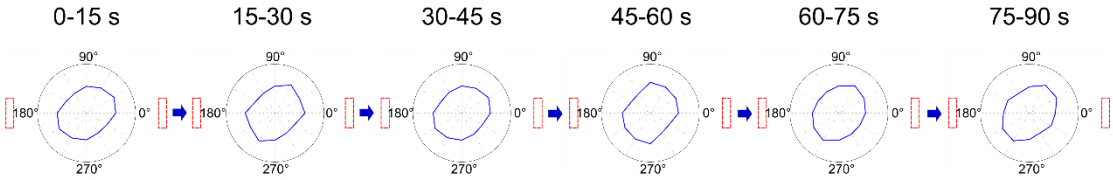

864

865

866 **Supplementary Figure S4. Radar plots of flies with suppressed P-ring neurons in**

867 **the post-stimulus stage**

868 (A) 32°C, *;;VT5404-GAL4, tub-GAL80^{ts}/ UAS-Kir2.1*.

869 (B) 32°C, *;;VT5404-GAL4, tub-GAL80^{ts}/ UAS-TNT*.

870

c105 > *CsChrimson* (no photoactivation)

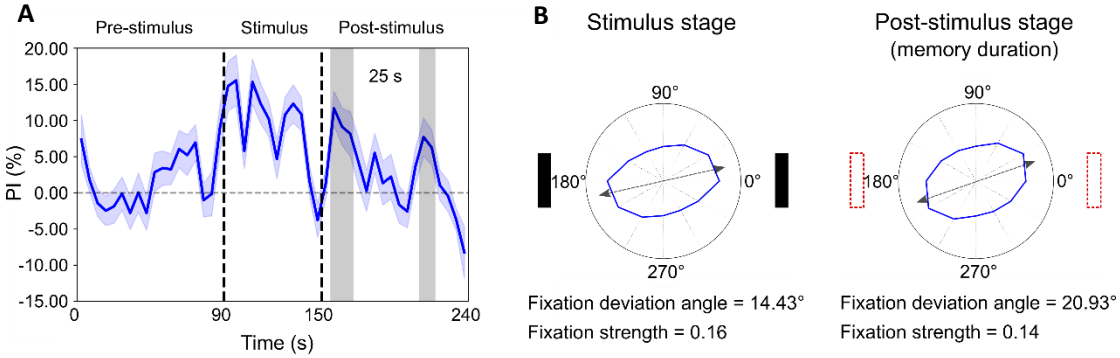

VT5404 > *CsChrimson* (no photoactivation)

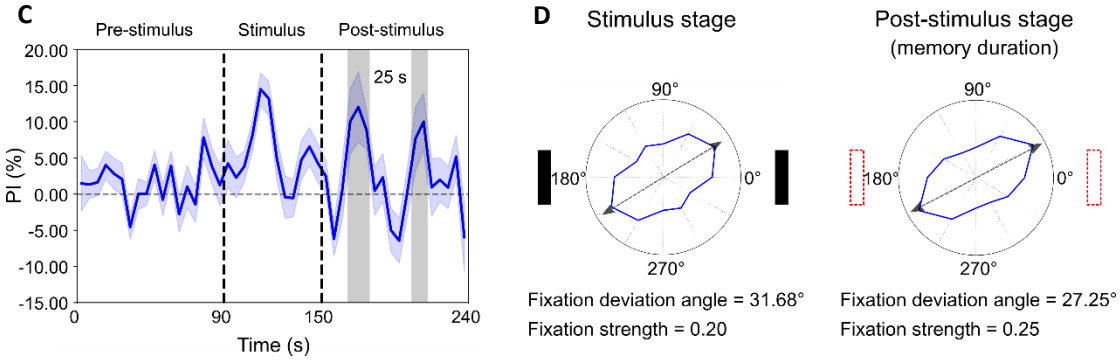

Supplementary Figure S5. Performance of control groups with the same types of transgenic flies used in the optogenetic experiments

(A) The performance index of flies carrying *c105-GAL4;;UAS-CsChrimson.mVenus* but no photoactivation was given during the whole task.

(B) The radar plots for the experiment shown in (A). during the stimulus stage (left) and the post-stimulus stage (right).

(C-D) Same as in (A-B) but with the flies carrying *;;VT5404-GAL4/ UAS-CsChrimson.mVenus*. Both control groups exhibited a similar fixation performance to that of the wild-type flies.

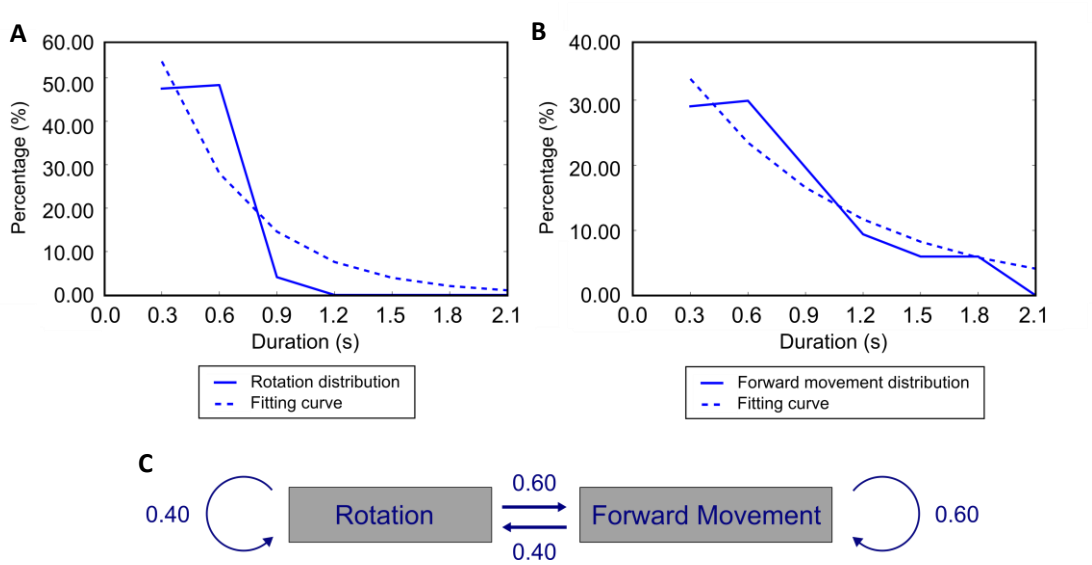

Supplementary Figure S6. Distributions of duration of different behavioral states and the Markov chain model of behavioral control。

(A) The distribution of duration of the rotation state. Dashed lines represent the fitting curves, which is given by $y = \alpha * \beta^{\frac{x}{0.3}}$. α is the fitting parameter and represents the probability of staying in the same state in each time window of 0.3 s. α = 0.471, β = 0.706 and R^2 = 0.778.

(B) Same as in (A) but for the forward movement state, α = 1.034, β = 0.521 and R^2 = 0.700. The exponential shape of the distribution of state duration indicates the Markov chain dynamics.

(C) The behavioral model was constructed based on the Markov chain dynamics and described the probability (given by the numbers next to the arrows) of a fly switching between behavioral states.

899 **Supplementary videos**

900 **Supplementary video S1. Laser escaping task for testing the visual perception of**
901 **the wild-type flies**

902 **Supplementary video S2. Laser escaping task for testing the visual perception of**
903 **the flies with suppressed P-ring neurons**

904 **Supplementary video S3. Laser escaping task for testing the visual perception of**
905 **the flies with deficient photoreceptors**

906 **Supplementary video S4. A representative trial of C-ring neuron photoactivation**
907 **during the last 30 s of the stimulus stage**

908 **Supplementary video S5. A representative trial of P-ring neuron photoactivation**
909 **during the last 30 s of the stimulus stage**

910

References

1. Valerio, S., and Taube, J.S. (2016). Head Direction Cell Activity Is Absent in Mice without the Horizontal Semicircular Canals. J. Neurosci. *36*, 741–754.
2. Yoder, R.M., and Taube, J.S. (2009). Head Direction Cell Activity in Mice: Robust Directional Signal Depends on Intact Otolith Organs. J. Neurosci. *29*, 1061–1076.
3. Hong, S.-T., Bang, S., Hyun, S., Kang, J., Jeong, K., Paik, D., Chung, J., and Kim, J. (2008). cAMP signalling in mushroom bodies modulates temperature preference behaviour in Drosophila. Nature *454*, 771.
4. Webb, B. (2019). The internal maps of insects. J. Exp. Biol. *222*, jeb188094.
5. Webb, B., and Wystrach, A. (2016). Neural mechanisms of insect navigation. Curr. Opin. Insect Sci. *15*, 27–39.
6. Lin, C.-Y., Chuang, C.-C., Hua, T.-E., Chen, C.-C., Dickson, B.J., Greenspan, R.J., and Chiang, A.-S. (2013). A comprehensive wiring diagram of the protocerebral bridge for visual information processing in the Drosophila brain. Cell Rep. *3*, 1739–1753.
7. Heisenberg, M., and Wolf, R. (2013). Vision in Drosophila: genetics of microbehavior (Springer-Verlag).
8. Robie, A.A., Hirokawa, J., Edwards, A.W., Umayam, L.A., Lee, A., Phillips, M.L., Card, G.M., Korff, W., Rubin, G.M., and Simpson, J.H. (2017). Mapping the neural substrates of behavior. Cell *170*, 393-406. e28.
9. Dewar, A.D., Wystrach, A., Philippides, A., and Graham, P. (2017). Neural coding in the visual system of Drosophila melanogaster: How do small neural populations support visually guided behaviours? PLoS Comput. Biol. *13*, e1005735.
10. Turner-Evans, D.B., and Jayaraman, V. (2016). The insect central complex. Curr. Biol. *26*, R453–R457.
11. Strauss, R. (2002). The central complex and the genetic dissection of locomotor behaviour. Curr. Opin. Neurobiol. *12*, 633–638.
12. Wolf, R., and Heisenberg, M. (1991). Basic organization of operant behavior as revealed in Drosophila flight orientation. J. Comp. Physiol. A *169*, 699–705.
13. Liu, G., Seiler, H., Wen, A., Zars, T., Ito, K., Wolf, R., Heisenberg, M., and Liu, L.

(2006). Distinct memory traces for two visual features in the Drosophila brain. Nature *439*, 551.

14. Muller, R.U., Ranck, J.B., and Taube, J.S. (1996). Head direction cells: properties and functional significance. Curr. Opin. Neurobiol. *6*, 196–206.
15. Su, T.-S., Lee, W.-J., Huang, Y.-C., Wang, C.-T., and Lo, C.-C. (2017). Coupled symmetric and asymmetric circuits underlying spatial orientation in fruit flies. Nat. Commun. *8*.
16. Turner-Evans, D., Wegener, S., Rouault, H., Franconville, R., Wolff, T., Seelig, J.D., Druckmann, S., and Jayaraman, V. (2017). Angular velocity integration in a fly heading circuit. eLife *6*, e23496.
17. Givon, L.E., Lazar, A.A., and Yeh, C.-H. (2017). Generating Executable Models of the Drosophila Central Complex. Front. Behav. Neurosci. *11*. Available at: http://journal.frontiersin.org/article/10.3389/fnbeh.2017.00102/full [Accessed August 11, 2017].
18. Constantinidis, C., and Wang, X.-J. (2004). A Neural Circuit Basis for Spatial Working Memory. The Neuroscientist *10*, 553–565.
19. Cope, A.J., Sabo, C., Vasilaki, E., Barron, A.B., and Marshall, J.A.R. (2017). A computational model of the integration of landmarks and motion in the insect central complex. PLOS ONE *12*, e0172325.
20. Green, J., Vijayan, V., Pires, P.M., Adachi, A., and Maimon, G. (2019). A neural heading estimate is compared with an internal goal to guide oriented navigation. Nat. Neurosci., 1.
21. Kim, S.S., Rouault, H., Druckmann, S., and Jayaraman, V. (2017). Ring attractor dynamics in the Drosophila central brain. Science *356*, 849–853.
22. Seelig, J.D., and Jayaraman, V. (2015). Neural dynamics for landmark orientation and angular path integration. Nature *521*, 186–191.
23. Green, J., Adachi, A., Shah, K.K., Hirokawa, J.D., Magani, P.S., and Maimon, G. (2017). A neural circuit architecture for angular integration in Drosophila. Nature *546*, 101.

24. Strauss, R., and Pichler, J. (1998). Persistence of orientation toward a temporarily invisible landmark in Drosophila melanogaster. J. Comp. Physiol. A Neuroethol. Sens. Neural. Behav. Physiol. *182*, 411–423.
25. Neuser, K., Triphan, T., Mronz, M., Poeck, B., and Strauss, R. (2008). Analysis of a spatial orientation memory in Drosophila. Nature *453*, 1244.
26. Götz, K.G. (1980). Visual guidance in Drosophila. Basic Life Sci. *16*, 391–407.
27. Yen, H.-H., Han, R., and Lo, C.-C. (2019). Quantification of Visual Fixation Behavior and Spatial Orientation Memory in Drosophila melanogaster. Front. Behav. Neurosci. *13*. Available at: https://www.frontiersin.org/articles/10.3389/fnbeh.2019.00215/full [Accessed September 14, 2019].
28. Fujiwara, T., Cruz, T.L., Bohnslav, J.P., and Chiappe, M.E. (2017). A faithful internal representation of walking movements in the Drosophila visual system. Nat. Neurosci. *20*, 72.
29. Humberg, T.-H., Bruegger, P., Afonso, B., Zlatic, M., Truman, J.W., Gershow, M., Samuel, A., and Sprecher, S.G. (2018). Dedicated photoreceptor pathways in Drosophila larvae mediate navigation by processing either spatial or temporal cues. Nat. Commun. *9*, 1260.
30. Wolff, T., Iyer, N.A., and Rubin, G.M. (2015). Neuroarchitecture and neuroanatomy of the Drosophila central complex: A GAL4-based dissection of protocerebral bridge neurons and circuits. J. Comp. Neurol. *523*, 997–1037.
31. Martín-Peña, A., Acebes, A., Rodríguez, J., Chevalier, V., Casas-Tinto, S., Triphan, T., Strauss, R., and Ferrús, A. (2014). Cell types and coincident synapses in the ellipsoid body of Drosophila. Eur. J. Neurosci. *39*, 1586–1601.
32. Ofstad, T.A., Zuker, C.S., and Reiser, M.B. (2011). Visual place learning in Drosophila melanogaster. Nature *474*, 204.
33. Pan, Y., Zhou, Y., Guo, C., Gong, H., Gong, Z., and Liu, L. (2009). Differential roles of the fan-shaped body and the ellipsoid body in Drosophila visual pattern memory. Learn. Mem. *16*, 289–295.

997 34. Thran, J., Poeck, B., and Strauss, R. (2013). Serum response factor-mediated gene
998 regulation in a Drosophila visual working memory. Curr. Biol. *23*, 1756–1763.
999 35. Guo, C., Du, Y., Yuan, D., Li, M., Gong, H., Gong, Z., and Liu, L. (2015). A conditioned
1000 visual orientation requires the ellipsoid body in Drosophila. Learn. Mem. *22*, 56–63.
1001 36. Shuai, Y., Hirokawa, A., Ai, Y., Zhang, M., Li, W., and Zhong, Y. (2015). Dissecting
1002 neural pathways for forgetting in Drosophila olfactory aversive memory. Proc. Natl.
1003 Acad. Sci. *112*, E6663–E6672.
1004 37. Eisel, U., Reynolds, K., Riddick, M., Zimmer, A., and Niemann, H. (1993). Tetanus
1005 toxin light chain expression in Sertoli cells of transgenic mice causes alterations of the
1006 actin cytoskeleton and disrupts spermatogenesis. EMBO J. *12*, 3365–3372.
1007 38. Sweeney, S.T., Broadie, K., Keane, J., Niemann, H., and O'Kane, C.J. (1995).
1008 Targeted expression of tetanus toxin light chain in Drosophila specifically eliminates
1009 synaptic transmission and causes behavioral defects. Neuron *14*, 341–351.
1010 39. Longden, K.D. (2016). Central brain circuitry for color-vision-modulated behaviors.
1011 Curr. Biol. *26*, R981–R988.
1012 40. Wu, M.-C., Chu, L.-A., Hsiao, P.-Y., Lin, Y.-Y., Chi, C.-C., Liu, T.-H., Fu, C.-C., and
1013 Chiang, A.-S. (2014). Optogenetic control of selective neural activity in multiple freely
1014 moving Drosophila adults. Proc. Natl. Acad. Sci. *111*, 5367–5372.
1015 41. Chang, H.-Y., and Ready, D.F. (2000). Rescue of photoreceptor degeneration in
1016 rhodopsin-null Drosophila mutants by activated Rac1. Science *290*, 1978–1980.
1017 42. Liske, E. (1977). The influence of head position on the flight behaviour of the fly.
1018 Calliphora erythrocephala. J. Insect Physiol. *23*, 375–379.
1019 43. Huang, Y.-C., Wang, C.-T., Su, T.-S., Kao, K.-W., Lin, Y.-J., Chuang, C.-C., Chiang,
1020 A.-S., and Lo, C.-C. (2019). A Single-Cell Level and Connectome-Derived
1021 Computational Model of the Drosophila Brain. Front. Neuroinformatics *12*. Available at:
1022 https://www.frontiersin.org/articles/10.3389/fninf.2018.00099/full [Accessed October
1023 17, 2019].
1024